International Journal of Automation and Computing

17(4), August 2020, 479-501
DOI: 10.1007/s11633-020-1225-4

A Survey on Modelling and Compensation for Hysteresis in High Speed Nanopositioning of AFMs: Observation and Future Recommendation

Maniza Armin[1] Priyo Nath Roy[2] Sajal Kumar Das[1]

[1] Department of Mechatronics Engineering, Rajshahi University of Engineering & Technology, Rajshahi 6204, Bangladesh

[2] Department of Mechatronics Engineering, Khulna University of Engineering & Technology, Khulna 9203, Bangladesh

Abstract: This paper surveys the recent advances on the modeling and control of hysteresis of piezoelectric actuators (PTAs) in the context of high precision applications of atomic force microscopes (AFMs). The current states, findings, and outcomes on hysteresis modeling and control in terms of achievable bandwidth and accuracy are discussed in detailed. Future challenges and the scope of possible research are presented to pave the way to video rate atomic force microscopy.

Keywords: Hysteresis, nonlinearities, piezoelectric actuator, smart actuator, atomic force microscope.

1 Introduction

Optimum performance and safety of mechanical structural systems are desired requirements in practical engineering applications[1–9]. In practice, most of the mechanical structures have some degree of non-linearities which have significant effect on optimum performance[10, 11]. These nonlinearity phenomena cause distortion or mismatch between input and output of that system. Depending on the degree of non-linearity and required performance of interest, some systems are treated as linear systems. However, in some practical cases like atomic force microscopes (AFM), scanning tunneling microscopy (STM), a small degree of non-linearity has significant effects on the performance of those systems. Hysteresis is considered as the most adverse non-linearities in piezoelectric actuators (PTAs)[12–17]. The hysteresis occurs when the output depends both on present and past inputs. It is the memory effect in magnetic and ferromagnetic materials[18–20]. In these materials, magnetization curve occurs in one direction and relaxation curve occurs in other direction when magnetizing field is removed and creates hysteresis loop. It is the simple lag between input u and output y in the u-y plane as shown in Fig. 1.

Hysteresis may cause several loops. The major loop is defined as the region where the output has multiple values within a range of $[-y, y]$ corresponding to the input range $[-u, u]$. The branch, output trajectory in u-y plane, which passes through major loop is called minor loop. The hysteresis loop indicates the hysteresis loss depending on the size of the hysteresis loop, and helps to select materials for making permanent magnet and core of machine by analyzing the value of retentivity. Higher hysteresis loop represents higher retentivity and coercivity of the material which is useful in hard disk drive, audio recording and credit cards applications[21].

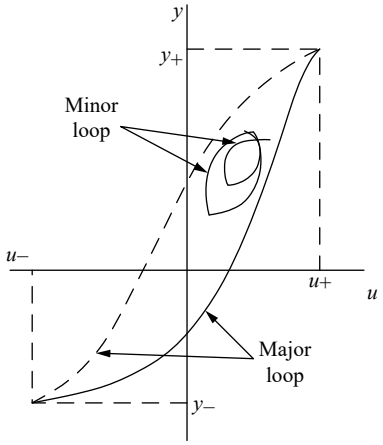

Fig. 1 Graphical representation of hysteresis obtained from [12]

The performance of the micro/nanoscanning systems depends on the accurate position of PTAs. The PTAs provide large bandwidth, high stiffness and unlimited displacement resolution[19, 22]. However, the output result of PTAs is not proportional to the excitation force[23]. When voltage is applied to the PTAs, it elongates but when voltage is removed, it does not trace the same path. This

Review
Manuscript received June 23, 2019; accepted January 20, 2020; published online April 14, 2020
Recommended by Associate Editor Zheng-Tao Ding

phenomenon has significant effects on nano-manipulating systems[6, 7].

The severity of the hysteresis in the PTAs depends on excitation. The intensity is directly proportional both to the amplitude and frequency of the excitation signal. The effects of hysteresis for image scanning in AFM is illustrated in Fig. 2 (a). The rectangular blocks in the images are required to follow the reference line. But due to hysteresis, the blocks deviate from reference line and distortion occurs in the resultant images. 15% position deviation of the total displacement range can occur due to hysteresis[24]. The position deviation bounds the implementation of scanning prob microscopy for long range scanning. In commercial application of AFM, high image scanning speed is required. But long time scanning produces hysteresis, which reduces the tracking accuracy and provides low quality scanning performance[25].

Creep effect is another nonlinearity of the PTAs that causes unwanted displacement in the scanning image over time which is shown in Fig. 2 (b). It is a result of low frequency signals and occurs when the AFM running in low operation range. In high speed operation, the creep nonlinearity is neglected[26, 27]. The creep is generated due to the continuous displacement of the PTA after removing the excitation signal which causes distortion in the scanning image of the AFM[28–30]. Generally, for slow speed operation of AFM, creep can be mitigated by designing a closed-loop control algorithm[31, 32].

The imaging performance of the PTAs for high speed operation also depends on precise controlling of mechanical vibration. However, low mechanical resonance frequency reduces the bandwidth. But at high operating speed while scanning the low resonant characteristics of the PTAs creates oscillatory displacement of the PTAs. The resonant mode of the PTAs which causes tracking error is created by applying a triangular signal in the X-axis. An effect is illustrated in Figs. 3 (a) and 3 (b) at two different frequencies which indicates that the images are more distorted at high frequencies.

The effect of hysteresis introduces a number of static and dynamic hysteresis models and control techniques of PTAs[2–5, 33–43]. Accurate modeling of PTAs provides significant position and tracking control. Modeling of hysteresis can be summarized into two ways: 1) physics-based model[44–46] and 2) mathematical-based model[40–43]. The physics-based models depend on material properties or physical principles. Implementation of the first principle is challenging because of unavailability of the material′s microstructure data. It may not be applicable to some practical problems. However, it is useful in designing of new material.

Consequently, the mathematical-based models are widely used to characterize wide class of hysteresis. These models are phenomenological in nature and are used to describe the microscopic structure by using experimental data. The Preisach model[40–43], Prandtl-Ishlinskii model[2–5, 33–35], Bouc-Wen model[36–39], Duhem model[47], thermal variable time relay hysteresis model, the Jiles-Atherton model, and the generalized Maxwell[6, 7] resistive capacitor-based lumped-parameter model are some phenomenology-based models which have been adapted to describe the characteristics of hysteresis. Their inversion models are then constructed to reduce hysteresis nonlinearity.

The non-linear static hysteresis can be described by a classical Preisach model (CPM)[40]. The hysteresis has two main properties, wiping-out and congruency property, that must be satisfied when modeling hysteresis. But CPM model only follows the wiping-out property. Moreover, application of classical Preisach model in the minor hysteresis loop will produce significant distortion. To overcome these limitations, modified generalized Pre-

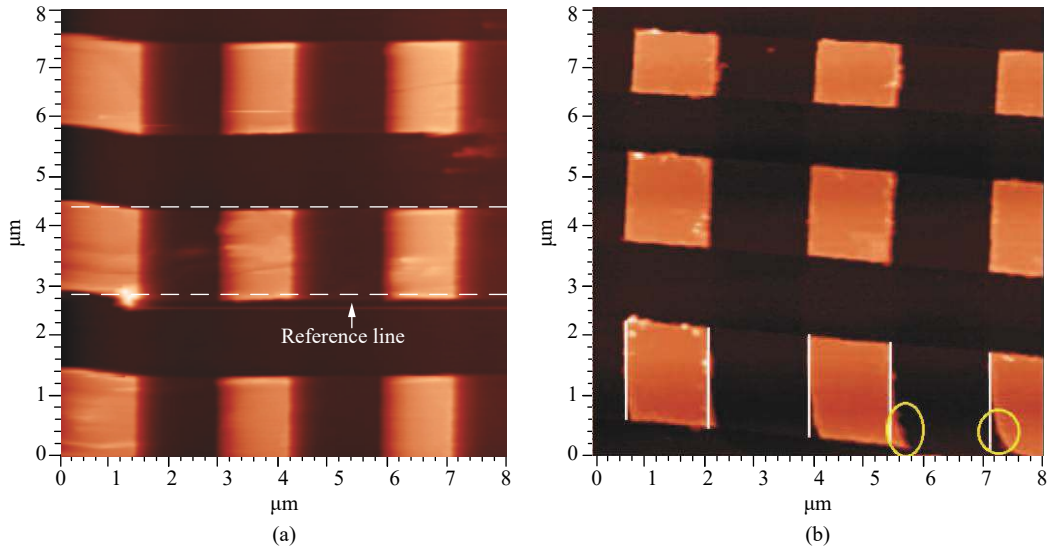

Fig. 2 Effect of non-linearities on scanned images: (a) Hysteresis effects on scanned image; (b) Creep effects on scanned image obtained from [12]

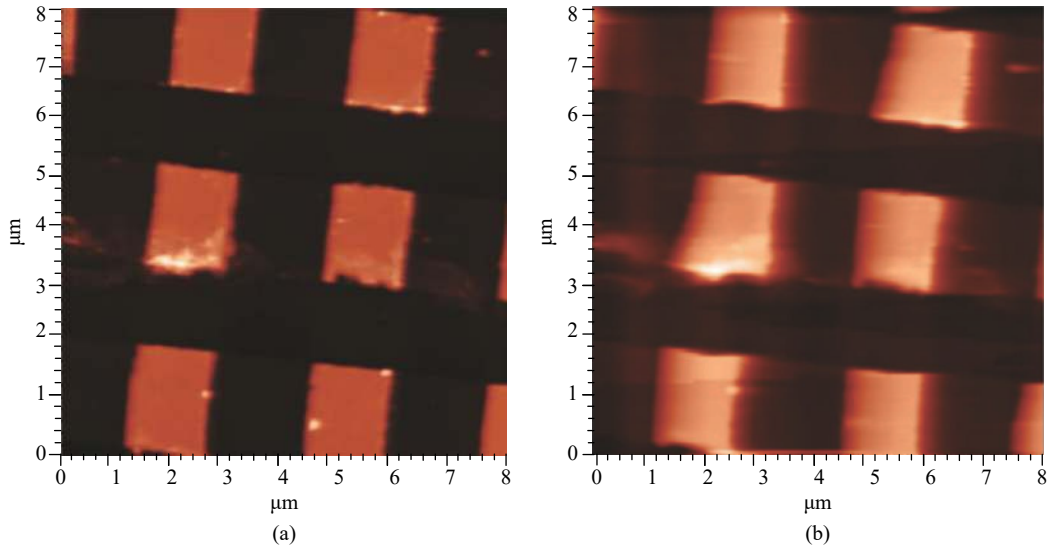

Fig. 3 Effect of cross coupling at (a) 15.62 Hz and (b) 62.5 Hz obtained from [12]

isach model is proposed for arbitrary types of input signals. However, these model are not practically invertible. The classical Prandtl-Ishlinskii model, subclass of CPM model, is introduced to overcome the limitations of the Preisach model[4]. It is the most widely used model which is analytically invertible. The classical P-I model consists of a family of play and stop operators. It is adapted for the modeling of symmetric and non-structured hysteresis. However, many modified P-I models are introduced for the modeling of rate-independent hysteresis and asymmetric rate-dependent hysteresis.

The Bouc-Wen model[36, 37] describes both hysteresis non-linearity and dynamics of the PTA using non-linear differential equations. It describes the symmetric hysteresis of the PTA while introduces wide class of hysteresis. It uses a few number of parameters for the implementation of this model. It was first introduced by Bouc in 1971. In 1976, Wen generalized it which is based on the consideration of mass-damper system with non-linear restoring force. As PTA possesses asymmetric hysteresis, modified Bouc-Wen model are used. The LuGre model, Coleman-Hodgdon model, Dahl model and the Maxwell-Slip model are the frictional physical based models[6, 7, 47]. The Duhem model which is a phenomenological explicit dynamic model, describes dynamic hysteresis based on differential equation. It is introduced by Pierre Duhem 1897 to characterize the hysteresis. It is the time derivative of the input signal. However, implementation of this model is complex because of the parameter identification complexity of its piecewise function.

The conventional and most commercial AFMs take several minutes to scan an image due to its slow scanning frequency. Due to higher scanning speed compared to the AFM′s operating speed, distortion occurs in the scanning image. To minimize the distortion of the scanning image, high operating speed AFM is required. But scanning at high frequency is a challenging task. For the achievement of high speed scanning AFMs, advanced control algorithms are developed and designed. But designing of controller for high speed AFMs introduces some challenges such as:

1) Scanning method. The optimal scanning method is the non-raster-scan method which requires further advancement.

2) Closed-loop bandwidth. For the AFM positioning accuracy, high closed-loop bandwidth is required.

3) Resonant mode. The AFMs are resonant system. So proper identification of resonant mode′s parameters is necessary.

4) Nonlinearity effects. Hysteresis, creep and their cross coupling effect. The controller must be robust over nonlinearity effects.

The above discussion clarifies that, the effect of hysteresis underpins the lack of performance of PTA when performing scanning at a high speed. Accurate modeling and control for compensation of hysteresis is necessary to achieve video rate atomic force microscopy.

In this paper, a brief of the models have been summarised to represent the dynamics effect of hysteresis in the context of high speed imaging of the AFM, then discussed accuracy of the models to capture measure data and investigate high accuracy models for hysteresis. Later, the details on control techniques to compensate for hysteresis are discussed broadly and confirms optimum controller in terms of achievable bandwidth. Finally, the paper is concluded with remarks of future work and recommendation.

2 Modeling of hysteresis

Fig. 4 depicts different types of hysteresis models that are used for the modeling of PTA′s hysteresis. The main goal of hysteresis modeling is to precisely characterises the system behaviors in terms of hysteresis. In this section, a detailed discussions on different hysteresis models

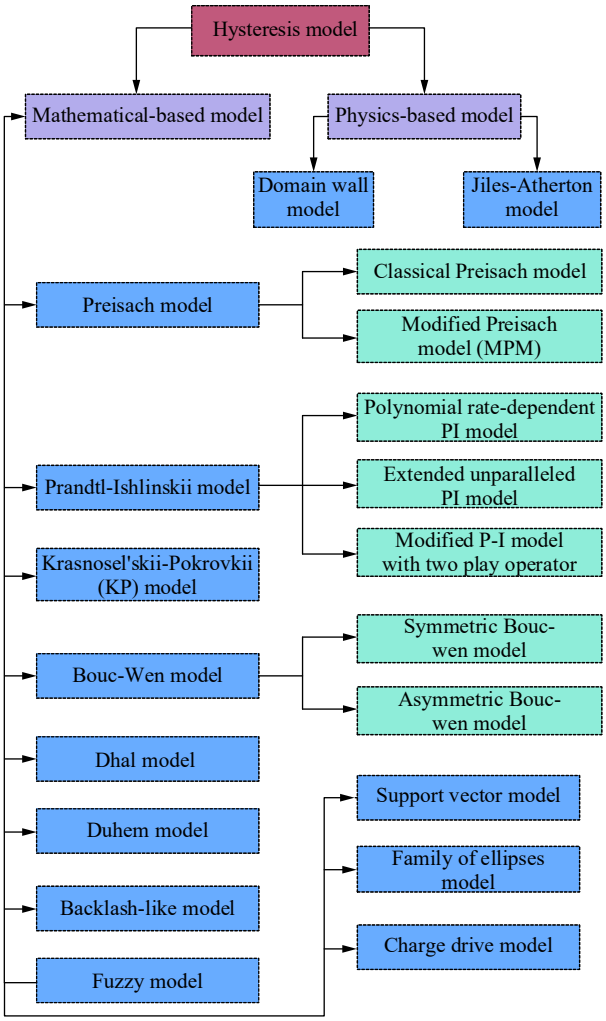

Fig. 4 Different types of hysteresis model

is presented.

2.1 Physics-based model

This type of models are material dependent and are complicated. The most widely known physics-based hysteresis model is Jiles-Atherton model (J-A) which was introduced to describe the ferromagnetic hysteresis[44, 45]. Based on these models, Smith and Ounaiesa introduced domain wall model[46] for this non-linearity. From J-A model, the relation between magnetization M and applied magnetic field strength H is defined as:

$$\frac{\mathrm{d}M}{\mathrm{d}H} = \frac{(1-c)(M_a - M_i)}{K\mathrm{sgn}(\dot{H}) - \delta(M_a - M_i)} + \frac{\mathrm{d}M_a}{\mathrm{d}H} \tag{1}$$

$$M_a = M_s\left(\coth\frac{1+\delta M}{a} - \frac{a}{1+\delta M}\right) \tag{2}$$

where M_a and M_i are defined as anhysteretic and irreversible parts respectively. The other parameters M_s, δ, a, c and K are linked nonlinearly.

Though physics-based model describes ferromagnetic hysteresis, model developed for one material may not be used for another material.

2.2 Mathematical-based model

Owing to the complexity of the physics-based models, in this section, a brief discussion on the Mathematical-based models are presented.

2.2.1 Preisach model

The simple and compact relative to other model is the classical preisach model (CPM)[40–43]. Because of its simplicity, it is widely used and provides fast algorithms to compensate hysteresis. Ferenc Preisach[34] first proposed this model as a mathematical model for the study of ferromagnetism. Due to its characteristics, it is only used for the purpose of describing the static hysteresis. The Preisach model consists of infinite number of continuous hysteron operators $\Psi_{\delta\lambda}[u(t)]$ which is shown in Fig. 5. The CPM has relay type two-state discontinuous operator $\Psi_{\delta\lambda}[u(t)]$ where δ and λ are acting as on and off thresholds with $\delta \geq \lambda$. $\Psi_{\delta\lambda}[u(t)]$ becomes $+1$ when the excitation $u(t)$ exceeds the threshold value of δ and becomes 0 when excitation $u(t)$ is less than threshold value of λ. However, the previous value retains if the excitation remains between the two thresholds value. More simply, the hysteron operator for PTA can be written as:

$$\Psi_{\delta\lambda}[u(t)] = \left\{ \begin{array}{ll} 1, & u(t) \geq \delta; \\ \Psi_{\delta\lambda}[u(t)], & \lambda \leq u(t) \leq \delta; \\ 0, & u(t) \leq \lambda. \end{array} \right\}.$$

This hysteron operator possesses the properties of the hysteresis where the output depends both on the extreme values in the current and past inputs. This is called memory effect. To produce wide range of reversal curves in the hysteresis loop on which accuracy of the CPM depends, the hysteron operator weighted with distribution function $\mu(\lambda, \delta)$. Mathematically, this model can be written as

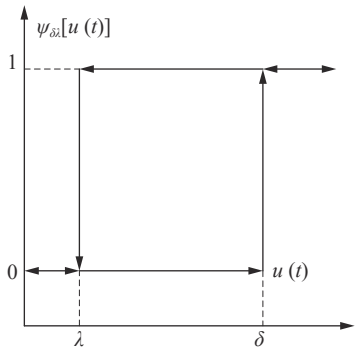

Fig. 5 Geometric representation of Relay operator

$$x(t) = P_p[u(t)] = \iint_{\delta \geq \lambda} \mu(\lambda, \delta) \Psi_{\delta\lambda}[u(t)] \mathrm{d}\,\delta\,\mathrm{d}\lambda \tag{3}$$

where $x(t)$ is defined as output displacement due to input voltage $u(t)$, $\Psi_{\delta\lambda}[u(t)]$ is the hysteron state and $\mu(\lambda, \delta)$ is the experimental distribution function.

The Preisach plane $(\delta - \lambda)$ facilitates to make the memory function. The geometric illustration of the equation in (3) is depicted in Fig. 6. In this plane,

$$p \triangleq \{(\delta, \lambda) \in p | \delta \geq \lambda,\ \lambda \leq \lambda_0, \delta \geq 0\},\ T(\delta, \lambda)$$

which is divided into s^- and s^+ surface. The s^- and s^+ are created when $\Psi_{\delta\lambda}[u(t)] = 1$ and 0, respectively.

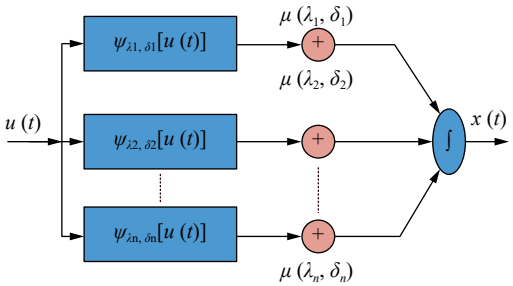

Fig. 6 Schematic representation of Preisach model

In the ascending loop of the hysteresis, the s^+ region increases from bottom to top and decreases from left to right in the descending loop. From wiping-out property of the CPM, the input history vanishes when the input $u(t)$ increases above or decrease below from the previous extremum. The increasing of input above the previous extremum prevents the hysteresis growth. The geometric interpretation in (3) can defined as follows:

$$x(t) = \iint_{s^+} \mu(\lambda, \delta) \Psi_{\delta\lambda}[u(t)] \mathrm{d}\delta\mathrm{d}\lambda + \iint_{s^-} \mu(\lambda, \delta) \Psi_{\delta\lambda}[u(t)] \mathrm{d}\delta\mathrm{d}\lambda. \tag{4}$$

For the PTA, it can be simplified as

$$x(t) = \iint_{s^+} \mu(\lambda, \delta) \mathrm{d}\delta\mathrm{d}\lambda \tag{5}$$

because of $\Psi_{\delta\lambda}[u(t)] = 1$ when $u(t) \geq \delta$ and $\Psi_{\delta\lambda}[u(t)] = 0$ when $u(t) \leq \lambda$.

As $u(t)$ varies from δ to λ, the output also changes which can be defined by Everett function:

$$X(\delta, \lambda) = \frac{1}{2}(x(\delta) - x(\delta, \lambda)) \tag{6}$$

which represents the output on the descending curve, δ is the maxima and λ is the minima of $u(t)$. Now, at points $x(\delta)$ and $x(\delta, \lambda)$, the Everett function shows that

$$x(\delta) = \iint_{s^+ + T(\delta,\lambda)} \mu(\lambda, \delta) \mathrm{d}\delta\mathrm{d}\lambda$$

$$x(\delta, \lambda) = \iint_{s^+} \mu(\lambda, \delta) \mathrm{d}\delta\mathrm{d}\lambda.$$

Rewriting above and taking into consideration, $X(\delta, \lambda)$ can be written as

$$X(\delta, \lambda) = \iint_{T(\delta,\lambda)} \frac{1}{2}(x(\delta) - x(\delta, \lambda)) \mathrm{d}\delta\mathrm{d}\lambda.$$

Similarly, the discrete CPM model can be expressed as

$$x(t) = \begin{cases} \Upsilon_1, \text{ if } & \dfrac{\mathrm{d}u(t)}{\mathrm{d}t} > 0 \\ \Upsilon_2, \text{ if } & \dfrac{\mathrm{d}u(t)}{\mathrm{d}t} > 0 \end{cases}$$

where

$$\Upsilon_1 = X(u(t), \delta_N) + \sum_{i=1}^{N} X(\delta_i, \lambda_{i-1}) - X(\delta_i, \lambda_i)$$

$$\Upsilon_2 = X(u(t), \delta_{N-1}) - X(\lambda_N, u(t)) + \sum_{i=1}^{N} X(\delta_i, \lambda_{i-1}) - X(\delta_i, \lambda_i)$$

where N defines the number of memorized extrema. For the description of the discrete Preisach model, the triangle $T(\lambda, \delta)$ split up into mesh. It contains $(\delta_i, \lambda_i) | i = 1, \cdots, N\ \ j = 1, \cdots, N$. The accurate hysteresis representation depends on the selection of N. Higher number of N provides higher accuracy of the hysteresis measurement.

Modified Preisach model (MPM)[48]: The limitations of the CPM model can be removed by using the modified Preisach model. This model adds a derivative term with the CPM and is written as follows:

$$x(t) = P_p[u(t)] - G_D \frac{\mathrm{d}u(t)}{\mathrm{d}t}$$

where $P_p[u(t)]$ is the CPM model and G_D is defined as derivative gain. G_D is used to decrease the error in the measurement in the hysteresis loop. Also, it describes the detachment phenomenon between major and minor hysteresis loops.

2.2.2 Prandtl-Ishlinskii model (PI)

The classical P-I model comprises of a family of hysteresis play or stop operator as shown in Fig. 7 and is widely used to capture the hysteresis effect[4]. The play operator possesses the rate-independent and symmetric hysteresis properties. As it is rate-independent function, it is influenced by both present and past input function $u(t)$. It was first introduced by Prandtl in 1928, as

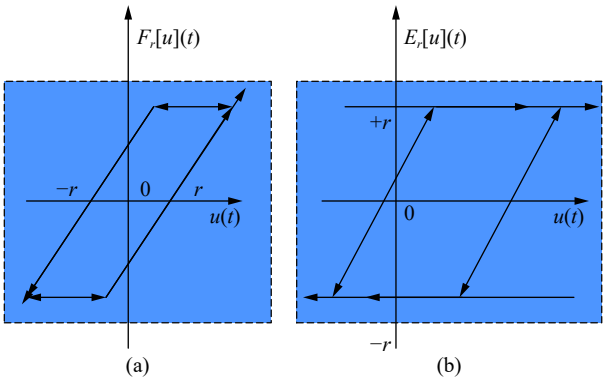

Fig. 7 Play and stop operators

$$y(t) = P_{dt}[u(t)] = P_0 u(t) + \int_0^{\Xi} P_r G_r[u](t)\mathrm{d}r \qquad (7)$$

where $u(t)$ and $y(t)$ are defined as input parameter and output parameter with respect to time, respectively. P_0 is defined as positive constant. r is the threshold with $r \in [0\ \Xi]$. $P(r)$ is the known density function with $P(r) > 0$ and $\int_0^{\infty} rP(r)dr < \infty$. $P(r)$ vanishes as r goes to infinite. $Gr[u]$ is the play operator.

Play operator: The play operator defines the width of the hysteresis loop. It relies on input $u(t)$ and threshold r such that

$$G_r[u](0) = g_r(u(0), 0)$$

$$G_r[u](t) = g_r(u(t), G_r[u](t_i))$$

for $t_i < t \le t_{i+1},\ 0 \le i \le N-1$ with $g_r[u,\ v] = \max(u - r, \min(u + r,\ v))$.

Here the time interval is $[0,\ t_N]$ with $0 = t_i < \cdots < t_N$, such that in every subinterval of $[t_i,\ t_{i+1}]$, the input $u(t)$ is monotone.

The P-I model can also be written as discrete form which is defined as

$$y(k) = P_{dt}[u](k) = P_0 u(k) + \sum_{i=1}^{N} P_i G_{ri} u(k)$$

where P_0 is the positive parameter and P_i is the weighted value. The classical play operator based P-I model describes only the symmetric rate-independent hysteresis. It does not describe the asymmetric hysteresis property of PTAs. These drawbacks of the classical P-I model are overcome by introducing various types of modified P-I model[1–3, 5, 16, 17, 19, 21, 33, 35, 49–53].

Polynomial rate-dependent P-I (PRPI) model[33]: The asymmetric behavior of the hysteresis is characterized by the PRPI model. Instead of using linear input function $P_0[u]$ of the classical P-I model, it uses polynomial with time rate input function. The PRPI model is defined as:

$$y(t) = P_{dt}[u(t)] = k_{p1}[u(t)] + k_{p2}\left[\frac{u(t)}{dt}\right] + \int_0^{\Xi} P_r G_r[u](t)\mathrm{d}r$$

where $k_{p1}[.]$ and $k_{p2}[.]$ are two odd functions.

Asymmetric shift P-I (ASPI) model[53]: The symmetric hysteresis described by classical P-I model is converted into asymmetric form by using a shift function. The saturated phenomenon is described by using auxiliary function along with P-I model. The ASPI model directly uses the available inverse results of PI model to construct an analytical form of it. It does not require the first order derivation and is able for describing asymmetric hysteresis. It does not provide precise parameter estimation but provides inverse compensation error. The ASPI model is written as

$$y(t) = P_{dt}[u](t) + P_{as}[u](t)$$

$$P_{as}[u](t) = R\Phi$$

where

$$\Phi = sat\left(\frac{\Psi[u]}{R}\right)$$

$$\Psi[u] = \Psi_1[u](t) + \Psi_2[u](t)$$

where R is defined as design parameter with $R > 0$. $\Psi_1[u](t)$ and $\Psi_2[u](t)$ are the shift model and auxiliary function, respectively. $P_{dt}[u](t)$ is the P-I model in (7). The saturation function $sat(\kappa)$ is given as

$$sat(\kappa) = \begin{cases} 1, & \text{if } \kappa > 1 \\ \kappa, & \text{if } -1 \le \kappa \le 1 \\ -1, & \text{if } \kappa \le -1 \end{cases}$$

and

$$\Psi_1[u](t) = \int_{m_0}^{m_1} P_{am}(m) G_m[u](t)\mathrm{d}m$$

where $P_{am} \ge 0$ is the density function with $\int_{m_0}^{m_1} mP_{am}(m)G_m\mathrm{d}m = l_{p_{am}} < \infty$ and $G_m[u](t)$ is the shift operator.

The play operator is written as

$$G_m[u](0) = g_m(u(0), 0)$$

$$G_m[u](t) = g_m(u(t), G_m[u](t_i))$$

for $t_i < t \le t_{i+1},\ 0 \le i \le N-1$ with

$$g_m[u,\ v] = \max(um,\ \min(u,\ v))$$

where m determines the shape of the shift operator; the time interval is $[0\ t_N]$ with $0 = t_i < t_2 < \cdots < t_N$. In every subinterval of $[t_i,\ t_{i+1}]$, the input $u(t)$ is monotone.

Generally, $G_m[u](t)$ is defined as left shift operator if $m > 1$ and right shift operator if $0 < m < 1$.

Extended unparalleled P-I (EUPI) model[54]: The EUPI model can capture a large range of hysteresis precisely. It uses a memoryless auxiliary function with UPI operator to describe the asymmetric hysteresis of the PTA. It is more capable of capturing complex hysteresis and relatively easier than generalized PI model to describe hysteresis.

UPI operator: The UPI operator is designed using classical P-I framework. A tilt factor is used to capture asymmetric hysteresis. It is given as

$$H_{r,\beta}[u](t) = \max\{u(t) - r,\ \min\beta(u(t) + r,\ v), H_{r,\beta}(\hat{t})\}$$

with $\hat{t} = \lim_{\delta\to 0+}(t - \delta)$ and $r \geq 0,\ \beta > 0$, where $u(t)$ is defined as input, r is dead zone and β is slope. Depending on β and r, the UPI operator becomes classical P-I operator when $\beta = 1$ and when $r = 0$, the UPI operator becomes shifted P-I operator. Based on the UPI operator, the EUPI model is written as

$$U_{PI}[u](t) = \int_{\underline{\beta}}^{\bar{\beta}} \int_0^{r_u} v(\beta, r) H_{r,\beta}[u](t) \mathrm{d}r\mathrm{d}\beta + P_{au}[u](t)$$

subjected to $v(\beta, r) \geq 0,\ \bar{\beta}, \underline{\beta}, r > 0$, where $v(\beta, r)$ is the density function, r_u is the dead zone of upper boundary, $P_{au}[u](t)$ is an auxiliary polynomial function and the tilt is defined in the range of $[\bar{\beta},\ \underline{\beta}]$. For the wiping out and congruency properties, the memory operators of EUPI model is defined as

$$H_{r,\beta}[u](t) = \iint_{m\leq n} \varphi(m, n)\varsigma_{m,n}[u](t)\mathrm{d}m\mathrm{d}n$$

where $\varsigma_{m,n}[u](t)$ and $\varphi(m, n)$ are the Preisach hysteron and density functions, respectively. Consequently, the discrete form of EUPI model is written as

$$U_{PI}[u](k) = \mu_1[u](k) + \mu_2[u](k) + P_{au}[u](k)$$

$$\mu_1[u](k) = \sum_i^{N_{\mu 1}} B_i H_{i,1} u(k) + A_0 u(k)$$

$$\mu_2[u](k) = \sum_i^{N_r} \sum_j^{N_a} D_{i,j} H_{ri,\beta j} u(k)$$

$$P_{au}[u](k) = \sum_i^{N_p} P_{(au)i} u(k) + P_{(au)0}$$

where A_0 is defined as linear gain with $A_0 > 0$, $r = 0$.

Modified P-I (MPI) model with two play operator: This hysteresis model consists of two play operator: 1) right side, and 2) left side.

Right side portion of the hysteresis loop is described by right side play operator consequently, left side portion is described by left side operator.

1) Right side play operator: For $0 < r < 1$, the right side operator $G_r^R[u](t)$ is described as

$$v(0) = G_r^R[u](0) = \int_r^R (u(0), 0, 1, 0)\mathrm{d}r$$

$$v(t) = G_r^R[u](t) = \int_r^R (u(t),\ G_r^R[u](t_i), \alpha(t),\ \beta(t))\mathrm{d}r$$

and the input function $u(t)$ is monotone with $u : [0, t_N] \to [0, 1],\ t_i < t < t_{i+1},\ 0 < i < N$, where

$$\int_r^R (u,\ v,\ \alpha,\ \beta)\mathrm{d}r = \max\{\frac{u - R}{1 - r}, \min(\alpha u + \beta,\ v)\}$$

$$\alpha(t) = \frac{v_M(t) - v_m(t)}{u_M(t) - u_m(t)}$$

$$\beta(t) = \frac{u_M(t)v_m(t) - u_m(t)v_M(t)}{u_M(t) - u_m(t)}$$

here, the input string is defined as $[u_M(t),\ u_m(t)]$ and the output string is defined as $[v_M(t),\ v_m(t)]$. These extrema have significant impact on the memory of the hysteresis.

Input/output string: Using the Madelung deletion rule, the maxima and minima of current input $u(t)$ and current output $v(t)$ is written as

$$u_M(t) = \min(s_{uM}(t))$$

$$u_m(t) = \max(s_{um}(t))$$

$$v_M(t) = \min(s_{vM}(t))$$

$$v_m(t) = \max(s_{vm}(t))$$

where the input maxima and minima are $s_{uM}(t)$ and $s_{um}(t)$, respectively. The output maxima and minima are $s_{vM}(t)$ and $s_{vm}(t)$, respectively.

2) Left side play operator: For $0 < r < 1$, the left side play operator $G_r^L[u](t)$ is written as

$$v(0) = G_r^L[u](0) = \int_r^L (u(0),\ 0,\ 1,\ 0)\mathrm{d}r$$

$$v(t) = G_r^L[u](t) = \int_r^L (u(t),\ G_r^L[u](t_i),\ \alpha(t),\ \beta(t))\mathrm{d}r$$

for $t_i < t < t_{i+1},\ 0 \leq i \leq N - 1$, where $\int_r^L (u,\ v,\ \alpha,\ \beta) = \max\{\frac{u}{1-r},\ \min\{\alpha u + \beta,\ v\}\}$.

Combining these two play operators, MPI model is written as

$$y(t) = P_{dt}[u](t) = P_0 u(t) + \int_0^{\Xi} P^R(r) G_r^R[u](t)\mathrm{d}r + \int_0^{\Xi} P^L(r) G_r^L[u](t)\mathrm{d}r$$

here, P_0 is the positive constant, $P^L(r)$ and $P^R(r)$ are left side and the right side density function, respectively. Similarly, the discrete form of the MPI model is written as

$$y(k) = P_{dt}[u](k) = P_0 u(k) + \sum_{i=1}^{N} P_i^R(r) G_{ri}^R[u](k) + \sum_{i=1}^{N} P_i^L(r) G_{ri}^L[u](k)$$

where P_i^R and P_i^L are the model parameters.

2.2.3 Bouc-Wen model

It describes both hysteresis non-linearity and dynamics of the PTA using differential non-linear equations. Basically, it describes the symmetric hysteresis of the PTA. As PTA possesses the asymmetric hysteresis, modified Bouc-Wen model are used[36, 37, 39]. It has the ability to describe a wide range of hysteresis.

Symmetric Bouc-Wen model[39]: If the state variable of PTA is y and the excitation is u, then from Bouc-Wen model, the relationship between u and y can be defined as

$$\dot{y} = A\dot{u}(t) - \lambda|\dot{u}|y|\dot{y}|^{n-1} - \lambda^{'}\dot{u}|y|^n$$

$$\dot{y} = \frac{\mathrm{d}y}{\mathrm{d}t},\ \dot{u} = \frac{\mathrm{d}u}{\mathrm{d}t}$$

where A is defined as the magnitude of the excitation, λ and $\lambda^{'}$ are used to control the shape and scale of the hysteresis, n is the transformation parameter.

Asymmetric Bouc-Wen model[36, 38]: An additional asymmetric operator is used with the Bouc-Wen model to characterise asymmetric hysteresis. The model is as

$$\dot{y} = A\dot{u}(t) - \lambda|\dot{u}|y(t)|\dot{y(t)}|^{n-1} - \gamma\dot{u}|y(t)|^n - \Psi u(t)\phi$$

where Ψ is the asymmetric operator, and

$$\phi = \mathrm{sgn}(\dot{u}(t)) = \begin{cases} 1, & \text{if } \dot{u}(t) > 0 \\ 0, & \text{if } \dot{u}(t) = 0 \\ -1, & \text{if } \dot{u}(t) < 0 \end{cases}$$

where the Bouc-Wen model parameters A, λ, γ and ϕ should be specified.

2.2.4 Dhal model[55, 56]

The second order Dhal model for the modeling of PTA hysteresis with state space representation is written as

$$\dot{v} = \alpha v\frac{\mathrm{d}x}{\mathrm{d}t} + \beta\varphi\frac{\mathrm{d}x}{\mathrm{d}t}$$

$$H = \gamma v$$

where x is the displacement in x-axis due to the applied excitation, v is the intermediate state vector, φ is the constant and

$$\alpha = \begin{bmatrix} 0 & 1 \\ \Omega_1 & -\mathrm{sgn}\left(\frac{\mathrm{d}x}{\mathrm{d}t}\right)\Omega_1 \end{bmatrix},\ \beta = \begin{bmatrix} 0 \\ 1 \end{bmatrix}$$

$$\gamma = \begin{bmatrix} \Psi_1 & \mathrm{sgn}\left(\frac{\mathrm{d}x}{\mathrm{d}t}\right)\Psi_2 \end{bmatrix},\ v = \begin{bmatrix} \Omega_1 & \Omega_2 \end{bmatrix}^{\mathrm{T}} = \begin{bmatrix} \Omega_1 \\ \Omega_2 \end{bmatrix}$$

where $\Omega_1 = \frac{2}{T}\ln\left(\frac{P_{n-1}}{P_n}\right)$

$$\Omega_2 = \left(\frac{2\pi}{T}\right)^2 + \left(\frac{\Omega_1}{2}\right)^2$$

$$\Psi_1 = G\Omega_2,\ \Psi_2 = s_0$$

where T is the time period, P_n is the n-th peak overshoot, G is the DC gain and s_0 is the initial slop.

2.2.5 Duhem model[57]

The Duhem hysteresis operator focuses on the changes in output with respect to the changes in input. Basically, it is used to characterise magnetic hysteresis since 1897[47, 58]. However, it has been adapted effectively to describe the piezoelectric hysteresis[57, 59]. It uses a differential equation or an integral operator to capture linear relation between input u and output y[58]. The differential equation of the Duhem model is as

$$\dot{y}(t) = f_1(y(t),\ u(t))\dot{u}_+(t) - f_1(y(t),\ u(t))\dot{u}_-(t) \tag{8}$$

where $\dot{u}_+(t) = \max[0,\ \dot{u}(t)]$ and $\dot{u}_-(t) = \min[0,\ u(t)]$. By using an integral operator, a simplified model of a particular case is given as

$$\dot{y}(t) + a|\dot{u}|g(u,\ y) = b\dot{u} \tag{9}$$

where g is defined as $g(u,\ y) = y - c\phi(u)$.

2.2.6 Backlash-like model[60, 61]

The Backlash-like model is a simplified form of Duhem model. The Backlash-like model is defined as

$$\dot{u}(t) = \rho|\dot{u}|[\sigma u - y] + B_1\dot{u} \tag{10}$$

where ρ, σ and B_1 are the constant with $\sigma > B_1$. The solution of (10) is expressed as

$$y(t) = \sigma u(t) + d(u(t)) \tag{11}$$

with $d(u(t)) = [y_0 - \sigma u_0]\mathrm{e}^{\rho(u-u_0)\mathrm{sgn}(\dot{u})} + \mathrm{e}^{-\rho u\mathrm{sgn}(\dot{u})} \times \int_{u_0}^{u}[B_1 - \sigma]\mathrm{e}^{\rho\xi\mathrm{sgn}(\dot{u})}\mathrm{d}\xi$, where $y_0 = y(0)$ and $u_0 = u(0)$ are

the initial condition for constant $\dot{u}$ and sgn is a sgn function.[60, 62–64].

2.2.7 Krasnosel′skii-Pokrovkii (KP) model[65]

The Krasnosel′skii-Pokrovkii (KP) model as shown in Fig. 8 consists of an elementary KP hysteresis operator[65]. The KP model is given as

$$y(t) = \Lambda[u(t)] = \iint_{\rho_2 \geq \rho_1} \mu(\rho_2, \rho_1) K_p[u,\ \xi(\rho)](t) \mathrm{d}\rho_2 \mathrm{d}\rho_1 \tag{12}$$

where $\mu(\rho_2, \rho_1)$ is the switching thresholds value with $\rho_2 > \rho_1$ and $K_p[u,\ \xi(\rho)](t)$ is the KP operator with

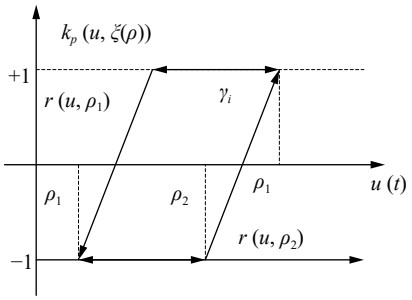

Fig. 8 Block diagram of the KP operator

$$K_p[u,\ \xi(\rho)](t) = \begin{cases} \max_{\rho \in P}\{\xi_0(\rho),\ r(u,\ \rho_2)\}, & \text{if } \dfrac{\mathrm{d}u}{\mathrm{d}t} > 0 \\ \min_{\rho \in P}\{\xi_0(\rho),\ r(u,\ \rho_1)\}, & \text{if } \dfrac{\mathrm{d}u}{\mathrm{d}t} < 0 \\ k_{p-}, & \text{if } \dfrac{\mathrm{d}u}{\mathrm{d}t} = 0 \end{cases}$$

$$\text{with } r(u,\ x) = \begin{cases} -1, & \text{if } \dfrac{\mathrm{d}u}{\mathrm{d}t} \leq 0; \\ -1 + \frac{2}{\alpha}(u - x), & \text{if } x < u < x + \alpha; \\ 1, & \text{if } u > x + \alpha \end{cases}$$

where $\rho = (\rho_1,\ \rho_2)$, $\alpha > 0$, k_{p-} indicates that KP operator remains unchanged and $\xi_0(\rho)$ is defined with $-1 \leq \xi_0(\rho) \leq 1$.

2.2.8 Other models

Besides the aforementioned models, a support vector machines[66], fuzzy systems[67], artificial neural networks[23, 68, 69], a family of ellipses models[31, 40, 70], charge drive model[71] have been developed. In addition, a phase shift model has been designed to capture the piezoelectric hysteresis[72]. Moreover, a polynomial based hysteresis models has been introduced to capture rate-independent hysteresis[18, 20, 73].

A summery of these hysteresis models is shown in Table 1. The above models have been implemented to precisely model the piezo-actuated stages in particular applications. But it is quite challenging to develop a generalized model for hysteresis nonlinearity of piezo-actuated stages.

3 Model identification method

This section deals with the dynamic model identification of the PTA system. The PTS system may be a simple input simple output (SISO) or a multiple input multiple output (MIMO) system. Usually, a swept sine wave is used for both SISO and MIMO cases as input through a high voltage amplifier to drive the piezoelectric tube actuator. The input is applied by using digital

Table 1 A brief summary of different types of hysteresis model

Techniques	References	Highlights
Preisach model (PM)	[40]	It describes the static hysteresis behaviour. They are not practically invertible and do not satisfy congruency property. It produces significant distortion on the minor loop. It does not provide sufficient information about actual hysteresis curve. Major and minor loop detachment is not considered in this model. Also, hysteresis model identification and implementation are very complex.
Prandtl-Ishlinskii model (PIM)	[74, 75]	The PI model is analytically invertible and more flexible in real time implementation. It does not describe the structured hysteresis behaviour. It is only used to model symmetric hysteresis.
Bouc-Wen model	[76, 77]	It provides less computation of its parameters and substantially reduces the cross-coupling effect. This model does not require any computation and model inversion to develop compensator. Moreover, the rate dependency and asymmetric hysteresis property are not described by this model. Also finding a general solutions of this model is quite challenging.
Dhal model	[55]	It describes asymmetric hysteresis better than Bouc-Wen model. Due to its less number of parameters, implementation of this model is very easy. Also it can capture dynamic model of hysteresis. The rate dependent property of the PTAs is not taken into account this model.
Backlash-like model	[60]	Backlash-like model is based on first-order differential equation and describes the dynamic hysteresis without modeling the inverse hysteresis. It is simpler than other hysteresis model and controller design is easier with this model. The drawback is its complexity to get a general solution of the model.
Krasnosellskii-Pokrovkii model (KP)	[65, 78]	The KP model is generally used to characterise the shape memory alloy actuator's hysteresis. The analytical inversion of the KP model is also complex.

signal analyzer. For the identification of SISO case, the input is applied along X-axis, and for MIMO case, both X-axis, and Y-axis are excited. The displacement of the PTA′s tip with respect to the excitation voltage is captured by using DSPACE control system. A system identification method is used to obtain the transfer function for X-axis and Y-axis dynamics of the PTS. The frequency response data are then analysed in Matlab toolbox to identify transfer function of the plant. In [22, 79], swept sine voltage from 10 Hz to 2 kHz were applied along X-axis and both X, Y-axis for SISO and MIMO system, respectively. The plant transfer function is identified using frequency response data. Fig. 9 represents the bode plot of the SISO PTS plant. To develop the LSVM model, a swept sine approach is used for the identification of the linear system[80]. The sine wave is generated to derive the piezoelectric tube bimorph with an amplitude of 0.5 V and frequency range of 1–1 000 Hz. A 2 Hz sampling rate is used to record the position response of the PTAs. In [52], a bandlimited noise signal is used in the system identification method which helps to characterise dynamics model of the system with sufficient accuracy. In some researches, black-box identification technique is used[81]. In this technique, the linear model is identified by selecting a specific point within an operating range over a prespecified bandwidth.

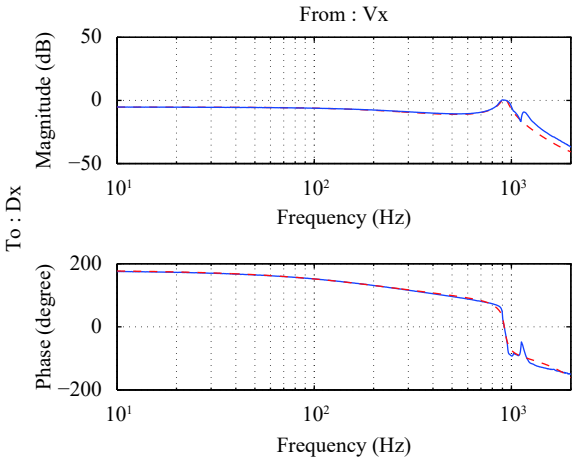

Fig. 9 Measured (the solid line) and identified model (the dashed line) frequency responses of PTS[79]

3.1 Modeling accuracy

The main motivation of modeling piezoelectric actuator is to precisely describe the nonlinearity behaviors. In Section 2, various types of models are used to describe the hysteresis non-linearity. Symmetric, asymmetric, rate-dependent and rate-independent hysteresis models are focused for the modeling of PTAs. Almost all the models have great precision and accuracy with a small modeling error, but their modeling accuraces are different with different working ranges. The most widely used Preisach model has an average tracking error which is 3%. Fig. 10 shows the comparison of modeling accuracy of different types of Preisach model. In 1995, Ge and Jouanech[82] adapted the classical Preisach model to characterise the hysteresis of PTAs. The maximum modeling error is 3% with a working range of 0–15 μm. But classical Preisach model produces a significant distortion when running on minor loop of the hysteresis output. To overcome this limitation, in 1997, they adapted a generalised Preisach model for this non-linearity in a new way[83]. It has a modeling error less than 2.7% with a tracking accuracy of 0.25 μm. The hysteresis non-linearity is also described by Preisach-type hysteresis model which is based on switching system concept[84]. The modeling error is 4 μm, i.e., 2% of the total displacement of 200 μm. In [85], a bilinear interpolation Preisach hybrid model was proposed with an error about 3.3% of the output displacement. Moreover, a modified Preisach model is proposed that has an error about 2% compared with the CPM with an error about 4%[48]. The Prandtl-Ishlinskii (PI) model is introduced to compensate the limitations of the Preisach model. For this purpose, a rate-dependent PI model is developed which has peak errors bounded between 3.57%–4.77% over a frequency range about 0.1–200 Hz[49]. In [17], a generalized PrandtlIshlinskii model is proposed. It has a peak position error near to 7.52%. Also the peak error is reduced to 2.43% using a feedforward control approach. However, in [86], a rate-dependent Prandtl-Ishlinskii model is proposed which has an ERMS of about 1.4% and maximum error of about 5.3%. The classical Prandtl-Ishlinskii model directly compensates the hysteresis error which is less than 2.5%[4]. Also a modified Prandtl-Ishlinskii model with a mean modeling error less than 1% is presented in [52]. In [53], an asymmetric shifted Prandtl-Ishlinskii (ASPI) model is developed which has modelling error less than 2.5%. A polynomial-based rate-dependent Prandtl-Ishlinskii (PRPI) model is introduced for characterising asymmetric hysteresis with root-mean-square error (ERMS) is about 0.6% and maximum is about 1.52%[33]. The modeling accuracy in terms of ERMS error is summarised in Fig. 11. It is noticed that PRPI model has a excellent modeling accuracy than other P-I models. However, the fractional-order Maxwell resistive capacitor model has maximum normalized root mean square error about 0.29% and an integrated physical model which uses Maxwell-slip elements has a maximum error about 0.93%[7, 87]. The Dahl model-based hysteresis compensator has modelling error about 4.2%[88]. In the Duhem mod-

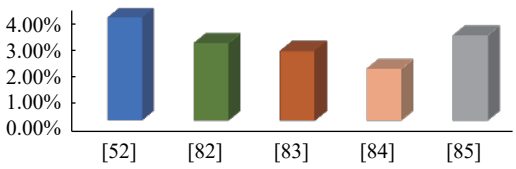

Fig. 10 Modeling accuracy of different types Preisach model

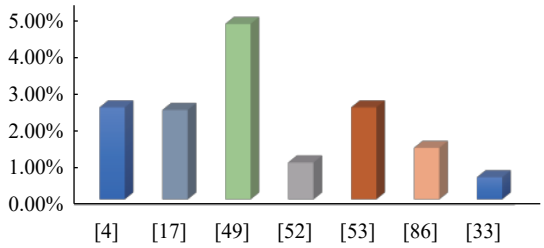

Fig. 11 Modeling accuracy of different types Prandtl-Ishlinskii models

el presented in [57], the ERMS is about 0.084 80 μm and the Bouc-Wen Model[37] has an error less than 2.5%.

Along with the aforementioned model, a simplified fuzzy based hysteresis model is introduced for capturing rate dependency and independency characteristics[89]. The maximum error and ERMS are 0.31% and 0.001 6, respectively. A neural network based hysteresis model has mean square error 0.010 27 and maximum error 0.061 7[68]. Instead of modeling inverse hysteresis compensator in feedforward loop, a least squares support vector machine (LSSVM)-based hysteresis model is introduced to compensate this non-linearity[80], but has ERMS error of about 0.15% and output position error about 0.50%. Moreover, an adaptive model is designed for characterising hysteresis nonlinearity[90]. The maximum error of the model is 0.036 3 and mean square error is 0.013.

The hysteresis modeling accuracy of different models are aggregated in Fig. 12. It is pointed out that the LSVM-based hysteresis model shows better modeling accuracy that of other hysteresis models.

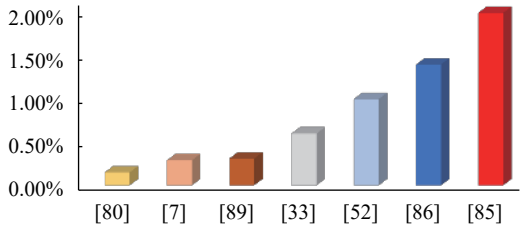

Fig. 12 Modeling accuracy of different types Hysteresis models

4 Control scheme of PTAs

In this section, various types of control algorithms are discussed for achieving of high tracking accuracy and nanopositioning requirements for different purposes. The main goal to control the PTAs is to mitigate the non-linear effects such as the hysteresis, creep and vibration. However, achievement of high speed scanning and precision positioning of PTAs stage is a challenging task. It is well known that scanning inaccuracy, oscillation and system instability are the phenomenon that are caused by hysteresis non-linearity. So, design and development of effective controller for controlling the hysteresis effect is a challenging task in the area of control system research.

However, many researchers have developed various control approaches over the past decades. The control approaches are classified into open-loop or feedforward control scheme and closed-loop control scheme. Further more, the closed-loop control scheme is divided into feedbackward (FB) control scheme and feedforward-feedback (FF-FB) control scheme. Through the literature review, these types of control approaches are described along with their tracking accuracy and closed-loop bandwidth.

The detailed of the aforementioned approaches will be discussed in the next section.

4.1 Open-loop control schemes of PTAs

The most used control approach is the feedforward control approach which is based on the hysteresis modeling and their inversion modeling as described in Section 2. A block diagram of the feedforward control scheme is shown in Fig. 13. Designing of open-loop control scheme has mainly two parts, 1) construction of the required hysteresis model, and 2) developing of feedforward controller.

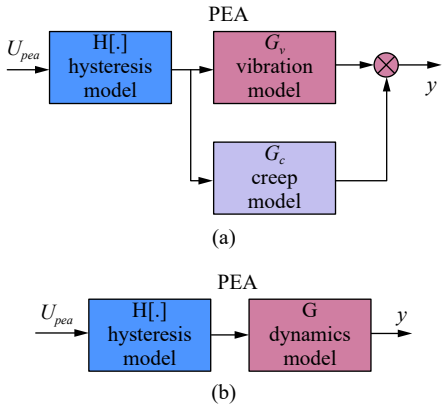

Fig. 13 A feedforward control architecture for PTAs

In the first approach, the feedforward compensators are designed by the adaptation of the direct hysteresis models[4, 21, 37, 42, 57]. For the need of high performance, easily computable and implementable control techniques and for avoiding use of bulky sensors, a feedforward controller using Bouc-Wen hysteresis model is developed[42]. It is based on multiplicative inverse structure. This provides less computation for designing the compensator. It utilizes direct model in designing the compensator. The main advantages of this model is the simplicity of computation and implementation. This prescribed model describes the static hysteresis but does not describe the dynamic one. Moreover, the traditional Bouc-Wen model is extended for multiple degree of freedom (DoF) systems[37]. The proposed model reduces the direct hysteresis less than 2.5% and substantially reduces the cross-coupling effect.

Based on the classical P-I model, an extended multiplicative-inverse structure is developed which reduces the

hysteresis less than 2.5% for the considered working frequency[4]. It also compensates the static hysteresis of the PTAs by constructing the compensator directly from the identified and obtained model. In [57], the generalized Duhem model (GDM) is adapted for the compensation of hysteresis nonlinearity of a biaxial piezo-actuated stage. The proposed GDM is a combination of the Duhem model, BoucWen model and Dahl model. The proposed feedforward controller effectively compensates the nonlinearities within a contouring error less than 0.1 μm.

In the second approach, the most widely used feedforward compensator requires inversion of the adapted hysteresis model. Among the models discussed in Section 2, Preisach and P-I models are operated based models from which inversion models are constructed. However, analytical inversion of the Preisach model is not possible. For this reason, various numerical methods are used for the inversion of the Preisach model[17, 41, 91–95].

The third approach is to develop a direct inverse hysteresis model without modeling the hysteresis effects[96]. The orientation of the hysteresis loop is different from those of the PTAs. Using this concept, the inversion of Preisach model is directly constructed[31]. Also the P-I model and modified P-I model for symmetric and asymmetric hysteresis compensation are used, respectively[33, 97].

However, modeling error, external loads and changes in the dynamic of PTAs will cause position inaccuracy of the feedforward control approach. To account this problem, disturbance-observer is used with the inverse MRC hysteresis model[51]. It is noted that the tracking accuracy and precession positioning of the PTAs is depended on the hysteresis modeling accuracy.

The feedforward (FF) control approach is used to manage complex hysteresis nonlinearities. But in all cases, the FF approach does not assure the stability of the entire model. To compensate these drawback, closed-loop control approaches are developed which is discussed in this section.

4.2 Closed-loop control schemes of PTAs

This control schemes are adapted both to mitigate the non-smooth hysteresis and to improve the performance of the PTAs. It can handle the parameter variations and disturbances as well as modeling uncertainties and nonlinearities. The challenging task is obtaining the robust stability in the feedback loop. Moreover, at high frequencies, tracking performance will degrade.

4.2.1 Feedback control schemes of PTAs

The feedback control schemes are widely used to compensate the modelling errors, variation in external loads, and dynamic model changes of the PTAs for the accurate position control. It is the most adaptable technique which guarantees the position control of the PTAs system. When the dynamics of the systems are unmodeled, it ensures the system's stability. Fig. 14 shows a typical feedback approach. In this approach, hysteresis nonlinearities are treated as uncertainties. Also the output y is forced to follow the desired output y_d. Based on the tracking performance error with unknown hysteresis, the practical implementation of the feedback controllers for dynamic systems is challenging[2, 5, 25, 50, 64, 98–103]. The feedback controller can be designed with or without the adaptation of hysteresis model. The former technique uses the known hysteresis models for capturing hysteresis behavior. In the later approach, the feedback controllers are designed directly without utilising the hysteresis models.

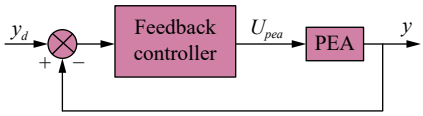

Fig. 14 Feedback control structure for PTAs

Estimation of any unknown disturbances in the PTAs system utilizing disturbance observer (DOB) compensator is known as a key idea of the later approach. However, to guarantee the tracking performance, additional feedback or feedforward controllers may be included in the system. In [56, 59, 104], various types of PID controllers, are used as a DOB compensator. In [59], the disturbance observer based proportional integral derivative (PID) controller compensates the hysteresis of the piezoelectric actuators under an input frequencies up to 150 Hz. An extended state observer is used as DOB with nonlinear PID controller in [56, 104]. However, precise tracking control is challenging by the classical PID controller as well as by the linear controllers due to phase lag problem. Considering this phase lag problem, a phase shift rate independent hysteresis model is constructed using the concept of Preisach model[72] and a variable phaser is designed to mitigate the minor hysteresis loop.

All the above controllers, state feedback, classical PID, are only used at low frequencies. To overcome these problems, many modern control techniques have been uesd by the researchers. In [81, 105, 106], a robust H_∞ feedback controller is used to mitigate the hysteresis effect. At high frequency scanning speed, the plant resonant behavior can be significantly compensated in this closed-loop system. Another simple and robust controller is the sliding mode controller[107–110]. To enhance the tracking performance against different types of uncertainties, an enhanced sliding mode motion tracking controller is adapted[107]. In [109], a disturbance observer is used to augment the sliding mode controller. Moreover, a discrete-time output integral sliding-mode controller (DOISMC) is constructed with two observers[110]. However, a PID based sliding mode controller (PIDSMC) with a PIDSM observer is combined to develop a PID-sliding-mode-observer-controller (PIDSMOC)[111]. It ensures an excellent tracking performance with small phase lag and error less than 3%. Though SM controller provides pro-

missing performance, accurate estimation of system parameters is challenging.

The incapability of sliding mode controller is overcome by adaptive controller, L_1 adaptive controller and an robust adaptive controller[19, 53, 63, 96, 112–118]. The development of the asymmetric shifted Prandtl-Ishlinskii (ASPI) model is based on PI model, a shifted model and an auxiliary function[53]. It directly uses the available inverse result of PI model to construct an analytical model of it. With this model, the adaptive approach is developed in feedback path for the enhancement of the closed-loop stability and for the mitigation of the compensation error. Moreover, a robust adaptive model reference controller is designed based on hysteresis-creep inversion technique[112]. In [98], an adaptive control approach is adapted for parameter estimation of PTAs. Also the integration of sliding mode controller with adaptive controller ensures the tracking accuracy under parametric uncertainties and uncertain nonlinearities. Moreover, combining the advantages of both SM and model predictive controller, a model predictive sliding mode controller has been reported in [119, 120].

A repetitive feedback controller has been designed based on the the Maxwell slip hysteresis model[121]. It improves the tracking accuracy for scanning images in PTAs. A fuzzy logic controller (FLC) with single-loop and dual-loop is presented in [122]. The mechanical resonance of the nanomanipulator is damped using integral resonant controller (IRC) with FLC. With this control shame, a better control is achieved in both x and y directions. In [66, 81, 105, 123], the hysteresis is treated as disturbance, and based on this phenomenon, various feedback controllers are designed.

Along with these, a gain schduling controller[124], a Smith predictor-based controller[125], neural network[126–128], fuzzy controller[129, 130], iterative controller[1, 131], linear-quardratic Gaussian (LQG) controller[132], linear-quardratic regular (LQR) controller[133], improve charge amplifier[15] and an active damping controller[134] have been used to achieve precision tracking of the scanner. In the next section, feedforward-feedback approach is discussed to mitigate the drawback of both feedforward and feedbak controller for the enhancement of tracking accuracy and loop stability.

4.2.2 Feedforward-feedback (Ff/Fb) control schemes of PTAs

Though both the feedforward and feedback controllers have great advantages, they alone are insufficient. The feedback controller is widely used to provide high-gain at low frequencies. But when frequency level is high, it provides low open-loop gain which is insufficient to compensate the hysteresis nonlinearities. Moreover, it is challenging for feedforward controller to have an accurate model due to parameter uncertainty. Thus, to overcome these problems, a combination of feedforward and feedback controller is used. Since feedforward-feedback controller is the combination of the advantages of the feedforward and feedback controllers, it improves the drawback of the feedforward and feedback controllers[6, 135]. A typical feedforward-feedback control scheme is represented in Fig. 15. Feedforward loop is used to improve the high-frequency performance where feedback controller is used to linearize the piezo-positioning systems or it is used to augment the feedback controller. Various types of hysteresis models are used for feedforward compensator to approximately compensate hysteresis and feedback loop is adopted for the reduction of the system modeling error and the system uncertainties[6, 10, 38, 40, 66, 91, 135–141]. In [10], the Preisach model was adapted in the feedforward path for hysteresis identification, and for feedback loop, a PID controller is used to reduce error and modeling uncertainties. Depending on PrandtlIshlinskii model, a compensator is designed as feedforward controller with repetitive feedback controller to increase the stability margin[139]. However, at high hysteresis non-linearities, where hysteresis is significant, the RC system becomes unstable. In [142], a modified Prandtl-Ishlinskii model is used for the modeling of asymmetric hysteresis of PTAs. Based on MPI model, an inverse hysteresis compensator is designed to capture this non-linearity. Moreover, a DOB is used to reject the disturbance. For precision tracking control, a proportional-integral controller is developed with DOB. The PIC+DOB+IHC control scheme reduces the hysteresis error about 80%.

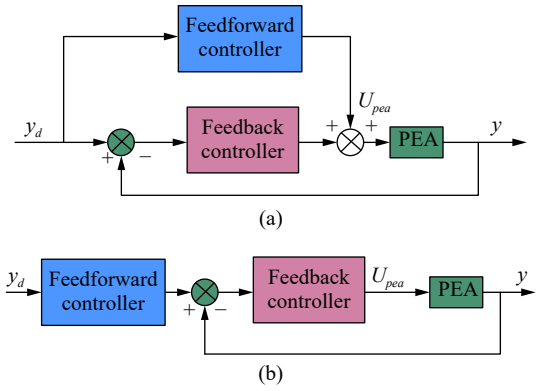

Fig. 15 Feedforward/feedback control scheme

In [66], a least squares support vector machines (LS-SVM) method is extended. To get control over the hysteresis model, the LSSVM model is trained using current input value and variation rate of the input. Based on inverse LSSVM model, a PID controller is combined with feedforward controller to suppress the hysteresis. The proposed model is simpler and more computationally efficient than standard SVM because it uses the equality constraints rather than inequality constraints. Moreover, it needs to tune fewer parameters.

A PrandtlIshlinskii model and its modified model is adapted in the feedforward loop for the compensation of

hysteresis[136, 143]. In [140], the feedforward compensator is combined with a robust H_∞ controller. The feedforward scheme reduces hysteresis where H_∞ controller ensures high performance. It provides a tracking error below 1%. The odd hysteresis non-linearity and disturbances are reduced using sliding mode controller[144]. The proposed control strategy produces 4 nm tracking resolution. An inversion-based model predictive controller (MPC) is used to reduce the hysteresis of the piezoelectric actuator[141]. The MPC controller is combined with an inverse feedforward control scheme and integral-of-error state variable. The adapted feedforward controller is simple than the Preisach model based inverse feedforward controller.

Many researchers have been used the feedforward-feedback controller for both hysteresis and vibration control[11, 24, 136, 145, 146]. In [145], modified PrandtlIshlinskii (MPI) model is adapted as feedforward control scheme to mitigate the asymmetric hysteresis nonlinearity. This direct inversion process reduces hysteresis error up to 81.35%. The feedback loop consists of a proportional-integral (PI) controller for creep non-linearity and uncertainty of the hysteresis and vibration modeling. It increases the bandwidth of the PTA system from 65 Hz to 605 Hz.

Also in [24], a linear integral resonant controller is used with the inverse MPI model for the compensation of both hysteresis and vibration of the the dynamic system. To enhance the tracking accuracy and closed-loop bandwidth, a tracking controller is designed as feedback controller. The proposed control scheme increases the closed-loop tracking bandwidth from 22 Hz to 657 Hz. In [146], a classical sky-hook controller is combined with feedforward controller. A robust H_∞ feedback controller is integrated with the feedfoward control scheme to mitigate both hysteresis and vibration of the PTA system[11]. The feedforward loop is adapted from the inversion of the Preisach model for hysteresis compensation.

A feedforward controller for hysteresis compensation and proportional integral (PI) controller for high speed raster scanning is implemented in [64]. It provides improved tracking performance when the frequency range is low. But, when the frequency range is high, it introduces phase lag between reference input and actual output. Therefore, at high frequencies, the proposed model does not provide satisfactory results for high speed raster tracking. In [6], a new control technique has been proposed to compensate hysteresis to achieve high tracking accuracy of the micromanipulator.

A PID controller with antiwindup strategy in the feedback path and an inverse Dahl model in the feedforward path is designed. It is simple and easy structure to implement for one or two dimensional tracking control. Above 700 Hz and 800 Hz frequency, the Ff/Fb approach does not provide precise results. This approach provides precise linear results losing bandwidth.

Based on inverse Maxwell resistive capacitor model, a feedforward control approach is developed for the augmentation of feedback controller[6]. The proposed controller provides precise linear results and enhances performance at high frequencies. In the feedback loop, a proportional-integral controller is designed to enhance the tracking performance at high frequencies. Feedback/feedforward control schemes provides faster response and smaller tracking errors about 0.12 μm. In [6], an asymmetric hysteresis of piezoelectric actuator is modeled through a modified Bouc-Wen model. For this purpose, a new digital inverse compensator with a simple structure cascaded in the feedforward path is designed. The modeling error and parameter uncertainties are eliminated by integrating the inverse controller with a PID feedback loop.

The static hysteresis of piezoelectric actuator is modeled through classical Preisach model[40]. The inversion of the Preisach model and a cascaded PD/leadlag feedback control approach is developed for precession control of PTAs. This approach is used for micropositioning control with both major and minor loop hysteresis compensations. It reduces the RMS error by 50% to 70%. Moreover, a rate-dependent feedforward control approach is derived and implemented from rate-dependent PrandtlIshlinskii (RDPI) model[91]. The Lipschitz continuity of the model is analyzed by bounding the tracking error. The feedforward control system is used to augment a feedback controller. The feedback controller reduces the remaining error and rejects disturbance that a feedforward controller would not eliminate. It provides infinite gain margin and larger phase margin compared to rate-independent Prandtl-Ishlinskii (RIPI) model.

Another feedforward-feedback controller is shown in Fig. 15 (b), where in feedback loop, a controller with high gain is used to compensate the uncertainties and non-linear effect. The feedforward controller is the inversion of the linear closed-loop dynamic model. It suppresses the computational error. However, zero-phase-error, zero-magnitude-error, and pre-filters like closed-loop stable inversion technique have also been developed for PTAs[147–151]. In this control approach, feedback path contains low gain margin problem.

Finally, Fig. 16 depicts different types of control approaches and Table 2 highlights the main control techniques.

4.3 Control accuracy

Based on the aforementioned control algorithms and approachs, the hysteresis control accuracy of the PTAs are different. Using the hysteresis model and their inverse model as feedforward control approach and different control algorithm as feedback approach, the tracking error of the piezoelectric tube stage is decreased to a acceptable range.

An inverse Preisach model in the feedforward loop and a hybrid controller with PID feedback is used for the

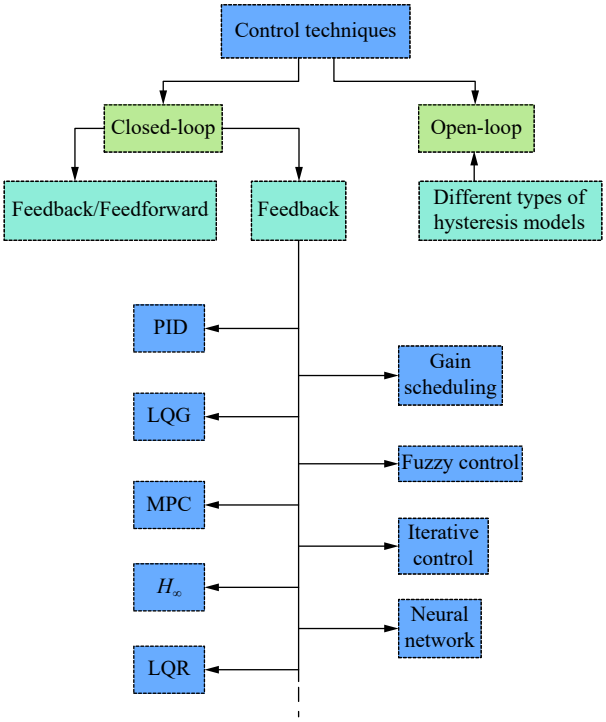

Fig. 16 Different types of control techniques for the control of PTAs hysteresis

compensation of hysteresis[94]. The average tracking error with this approach is 36 nm. In [40], an inversion hysteresis model derived from classical Preisach model is used for the compensation of hysteresis. To improve the control accuracy, a cascaded PD/lead-lag controller is combined with various types of hysteresis model. This approach has a maximum tracking error about 2.5 µm. A PD type feedback controller is integrated with a feedforward switching-type asymmetric hysteresis model that has a average tracking error about 0.68 µm[84]. In [11], a H_∞ controller is used in the feedback loop with Preisach model in the feedforward loop. This control approach has a root mean square error about 0.262 µm to track 10 µm triangle trajectory.

A proportional integral (PI) feedback controller is combined with model-based inversion feedforward control approach for the compensation of hysteresis and for achieving precise tracking accuracy[152]. This type of composite approach achieved a closed loop bandwidth of 70 Hz and precision accuracy about 0.281 µm. Based on ellipse-based hysteresis model, an inverse based hysteresis compensator is developed for rate-dependent hysteresis[31]. A hybrid control scheme is designed by integrating a PID controller with the hysteresis model in the feedforward loop. From experiment, it is evident that the tracking error is less than 0.1 µm, which is 0.7% of the moving range. Furthermore, a real-time feedforward controller is designed with the proposed hysteresis model[70]. It produces a maximum tracking error 0.08 µm which is 1.52% of the 18 µm displacement range. The Maxwell resistive capacitor model is designed as a feedforward hysteresis compensator and a proportional integral feedback controller is combined with the proposed hysteresis model[135]. The feedback/feedforward control scheme has a small tracking error about 0.12%. In [80], a least squares support vector machine (LSSVM)-based hysteresis model reduces the RMS tracking error to a level of 0.62 µm.

The most widely used hysteresis compensator model is the Prandtl-Ishlinskii (PI) model. By using inverse PI model in the feedforward loop, the effect of the hysteresis nonlinearity is reduced[144]. Then, a sliding controller is designed in the feedback loop, to mitigate the remaining hysteresis. The proposed control approach has a closed loop bandwidth about 80 Hz and a maximum tracking error 0.039 µm. Also a repetitive controller is designed with RMS error about 1.38%[139]. A rate dependent feedforward controller is designed with PI hysteresis model which has mean RMS error about 0.094 3 µm with maximum error about 0.389 9 µm[143]. In [153], a modified PI model is cascaded with a feedforward controller which has an error below 1%. Also, the inversion of the MPI hysteresis model is used with a feedback proportional integral controller which produces root-mean-square tracking error about 0.007 2%[145]. The proposed closed loop control system has a bandwidth from 65 Hz to 605 Hz.

Moreover, to improve the closed loop bandwidth, an integral tracking controller (ITC), an integral resonant controller (IRC), and a feedforward controller is cas-

Table 2 Highlights of different types of control approaches

Techniques	Highlights
Feedforward (Ff) control scheme	The feedforward controllers are constructed by cascading different types of hysteresis models and their inverse models. It utilizes known dynamic models of the system for the control input. It improves the control performance of the PTAs. But, alone FF controller can not improve the tracking accuracy. Moreover, due to parameter uncertainty, it is quite challenging to have a accurate model.
Feedback control (Fb) scheme	The feedback control scheme eliminates the remaining hysteresis by using robust control algorithm. It guaranties robust tracking performance under nonlinearities, unmodeled dynamics, parameter variations and uncertainties. It provides high open loop gain at low operating frequencies. However, its implementation is difficult and sophisticated and needs bulky sensors for output signal. It becomes complex to design a feedback controller for high operating frequencies. Also, stability in the control loop is the most important thing in designing feedback controller.
Feedback/Feedforward (Ff/Fb) control scheme	The Ff/Fb controller holds the advantages of feedforward and feedback controller. It is implemented to get high precession and high operating speed of piezo-actuated stages.

caded with inverse hysteresis compensator based on modified PI model[24]. The closed loop tracking bandwidth is 657 Hz and RMS tracking error is about 8.6 nm, i.e., 0.008 6 μm. In [154], a PI controller is integrated with Smith predictor and input shaper. It achieves a closed loop bandwidth at a range about 22.6 Hz to 510 Hz and tracking error about 0.056 9 μm. Also, a proportional integral controller (PIC) and a disturbance observer are designed with the inverse modified Prandtl-Ishlinskii model[142]. It accounts a RMS tracking error about 0.027 8 μm. In [21], inversion of the CPI model is adapted in the feedforward loop with a H_∞ feedback controller to compensate hysteresis effect. It provides a closed loop bandwidth 67 dB and RMS tracking error 0.814 μm under 1 Hz applied frequency. Also, a full-order and fixed-order H_∞ feedback control approach is develoed to mitigate the remaining hysteresis[140]. The full-order H_∞ controller provides a fine tracking accuracy with RMS error about 0.09 μm. With the PI model, an adaptive controller is used with a tracking error 0.080 4 μm[19].

The summarised control accuracy of different control approaches is represented in Fig. 17. Among the control approaches it is noted that the ITC+IHC+IRC+FFI controller[24], provides better tracking accuracy of the scanning images. It provides high scanning speed and high-precision performances than the other control approaches.

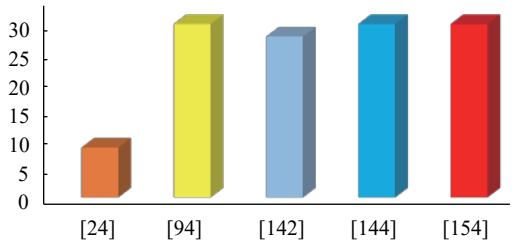

Fig. 17 Control accuracy of different types of control algorithm

However, there are many feedback controllers which are used to achieve better tracking accuracy without using hysteresis modeling. For high-precision positioning, a LQG controller is designed which is integrated with augmented plant model[155]. This closed loop control approach provides high quality image up to 120 Hz scanning frequency with a RMS tracking error about 10.32 nm. Using the sliding mode control scheme, the bandwidth of closed loop system is improved by 88 Hz and provides a tracking error about 3.6% of the maximum amplitude[156]. In [118], a PID-based sliding mode controller is designed. It has an excellent tracking accuracy with the maximum tracking error less than 3%. A cerebellar model articulation controller (CMAC) is designed based on neural network control algorithm[126]. It has a tracking resolution about 2 nm. When plant parameter uncertainties are absent, an inversion-based feedforward control technique is more compatible to achieve the tracking accuracy of the PTAs[150]. It improves the closed loop bandwidth 310 Hz to 1 320 Hz with a tracking error about 5% of 100 Hz scanning frequency. In [157], a high-bandwidth and high tracking resolution XY nano-positioning stage are developed. To increase the tracking accuracy and bandwidth, a proportional integral control algorithm is implemented. The proposed controller increased the closed loop bandwidth about 2 000 Hz with a tracking resolution about 1nm. However, for enhancing the flexibility of the AFM imaging accuracy, some local data are used to compensate hysteresis effect[158,159].

The aforementioned modelling and control approaches for hysteresis mentioned in this paper are also related to other positioning systems other than AFMs. Such nanopositioning systems are scanning probe microscopy (SPM)[160], ultra-precision machine tools[161], micromanipulators[162], piezoelectric actuator drive (PAD) and hard disk drive[163], etc. However, there are many new advanced control algorithms which can be used for controlling purpose of AFMs[164–167].

5 Conclusions & future recommendations

The high speed nano-positioning of PTA has been an area of active research for decades now. The control of PTA based on hysteresis modelling has attracted the researchers for high level of accuracy of hysteresis modeling. This paper investigates the merit of seven hysteresis models that are used for control of piezo-electric actuator in high speed nano-positioning. The investigated models are summarised in terms of tracking accuracy for command signals. The investigation shows that Bouc-Wen model is simple to obtain, however least square support vector machine based hysteresis model has higher accuracy as compared to other models presented in this paper.

Moreover, to improve the tracking accuracy at high frequencies, different types of feedback and feedforward controllers, such as PID, LQG, LQR, H_∞, ITC, MPC, fuzzy controller, neural network, etc. are used. The investigation summarises the control accuracy of these controllers. Aforementioned discussion concluded that PID controller is versatile and simpler than other controllers, but among them, the combination of ITC+IHC+IRC+FFI controller provides better tracking accuracy of the scanned image.

Finally, this survey paper concluded with the following future recommendation:

1) Though the raster scanning method is widely used, it takes several times and damages the sharp tip of the scanning images. Moreover, raster scanning tracks the triangular signal and produces vibration on the scanning tip. For the improvement of these problems, non-raster scanning method can take the place of the conventional raster scanning method.

2) Adaptive artificial control algorithms can be used in terms of conventional control approach to improve the

tracking accuracy at high speed operating range.

3) When scanning images at high frequencies, the feedback control approach provides low closed loop bandwidth. Also, feedforward control approach has some limitations such as instability of the entire model. For the improvement of the tracking accuracy and closed loop bandwidth at high frequencies, inverse feedforward control approach can be used with the combination of feedforward/feedback control approach.

4) Moreover, modern technology included AFM such as artificial intelligent AFM can be used for getting better scanning results.

5) The hysteresis of an AFM is not only from the piezoelectric actuators but also from the mechanical mechanisms. Therefore, the control system should consider the hysteresis of the mechanical mechanism.

References

[1] Y. Wu, Q. Z. Zou. Iterative control approach to compensate for both the hysteresis and the dynamics effects of piezo actuators. *IEEE Transactions on Control Systems Technology*, vol. 15, no. 5, pp. 936–944, 2007. DOI: 10.1109/TCST.2007.899722.

[2] X. Y. Zhang, Y. Lin, J. Q. Mao. A robust adaptive dynamic surface control for a class of nonlinear systems with unknown Prandtl-Ishilinskii hysteresis. *International Journal of Robust and Nonlinear Control*, vol. 21, no. 13, pp. 1541–1561, 2011. DOI: 10.1002/rnc.1652.

[3] Z. Y. Sun, B. Song, N. Xi, R. G. Yang, L. N. Hao, Y. L. Yang, L. L. Chen. Asymmetric hysteresis modeling and compensation approach for nanomanipulation system motion control considering working-range effect. *IEEE Transactions on Industrial Electronics*, vol. 64, no. 7, pp. 5513–5523, 2017. DOI: 10.1109/TIE.2017.2677300.

[4] M. Rakotondrabe. Classical Prandtl-Ishlinskii modeling and inverse multiplicative structure to compensate hysteresis in piezoactuators. In *Proceedings of American Control Conference*, IEEE, Montreal, Canada, pp. 1646–1651, 2012. DOI: 10.1109/ACC.2012.6314620.

[5] C. Y. Su, Y. Feng, H. Hong, X. K. Chen. Adaptive control of system involving complex hysteretic nonlinearities: A generalised Prandtl-Ishlinskii modelling approach. *International Journal of Control*, vol. 82, no. 10, pp. 1786–1793, 2009. DOI: 10.1080/00207170902736307.

[6] Y. F. Liu, J. J. Shan, U. Gabbert. Feedback/feedforward control of hysteresis-compensated piezoelectric actuators for high-speed scanning applications. *Smart Materials and Structures*, vol. 24, no. 1, Article number 015012, 2014. DOI: 10.1088/0964-1726/24/1/015012.

[7] Y. F. Liu, J. J. Shan, U. Gabbert, N. N. Qi. Hysteresis and creep modeling and compensation for a piezoelectric actuator using a fractional-order maxwell resistive capacitor approach. *Smart Materials and Structures*, vol. 22, no. 11, Article number 115020, 2013. DOI: 10.1088/0964-1726/22/11/115020.

[8] S. K. Das, H. R. Pota, I. R. Petersen. Multivariable negative-imaginary controller design for damping and cross coupling reduction of nanopositioners: A reference model matching approach. *IEEE/ASME Transactions on Mechatronics*, vol. 20, no. 6, pp. 3123–3134, 2015. DOI: 10.1109/TMECH.2015.2411995.

[9] S. K. Das, H. R. Pota, I. R. Petersen. Damping controller design for nanopositioners: A mixed passivity, negative-imaginary, and small-gain approach. *IEEE/ASME Transactions on Mechatronics*, vol. 20, no. 1, pp. 416–426, 2015. DOI: 10.1109/TMECH.2014.2331321.

[10] P. Ge, M. Jouaneh. Tracking control of a piezoceramic actuator. *IEEE Transactions on Control Systems Technology*, vol. 4, no. 3, pp. 209–216, 1996. DOI: 10.1109/87.491195.

[11] P. J. Ko, Y. P. Wang, S. C. Tien. Inverse-feedforward and robust-feedback control for high-speed operation on piezo-stages. *International Journal of Control*, vol. 86, no. 2, pp. 197–209, 2013. DOI: 10.1080/00207179.2012.721568.

[12] S. K. Das, H. R. Pota, I. R. Petersen. Intelligent tracking control system for fast image scanning of atomic force microscopes. *Chaos Modeling and Control Systems Design*, A. T. Azar, S. Vaidyanathan, Eds., Cham, Germany: Springer, pp. 351–391, 2015. DOI: 10.1007/978-3-319-13132-0_14.

[13] G. Aguirre, T. Janssens, H. van Brussel, F. Al-Bender. Asymmetric-hysteresis compensation in piezoelectric actuators. *Mechanical Systems and Signal Processing*, vol. 30, pp. 218–231, 2012. DOI: 10.1016/j.ymssp.2011.11.012.

[14] D. An, H. D. Li, Y. Xu, L. X. Zhang. Compensation of hysteresis on piezoelectric actuators based on tripartite PI model. *Micromachines*, vol. 9, no. 2, Article number 44, 2018. DOI: 10.3390/mi9020044.

[15] D. Amin-Shahidi, D. L. Trumper. Improved charge amplifier using hybrid hysteresis compensation. *Review of Scientific Instruments*, vol. 84, no. 8, Article number 085115, 2013. DOI: 10.1063/1.4818140.

[16] O. Aljanaideh, M. Rakotondrabe, H. Khasawneh, M. Al Janaideh. Rate-dependent Prandtl-Ishlinskii hysteresis compensation using inverse-multiplicative feedforward control in magnetostrictive terfenol-d based actuators. In *Proceedings of American Control Conference*, IEEE, Boston, USA, pp. 649–654, 2016. DOI: 10.1109/ACC.2016.7524987.

[17] M. Al Janaideh, S. Rakheja, C. Y. Su. An analytical generalized Prandtl-Ishlinskii model inversion for hysteresis compensation in micropositioning control. *IEEE/ASME Transactions on Mechatronics*, vol. 16, no. 4, pp. 734–744, 2011. DOI: 10.1109/TMECH.2010.2052366.

[18] S. Chonan, Z. W. Jiang, T. Yamamoto. Nonlinear hysteresis compensation of piezoelectric ceramic actuators. *Journal of Intelligent Material Systems and Structures*, vol. 7, no. 2, pp. 150–156, 1996. DOI: 10.1177/1045389X9600700205.

[19] Y. S. Chen, J. H. Qiu, J. J. Wu. Adaptive control with hysteresis compensation for piezoelectric actuators. *International Journal of Applied Electromagnetics and Mechanics*, vol. 52, no. 1-2, pp. 843–850, 2016. DOI: 10.3233/JAE-162229.

[20] C. H. Ru, L. N. Sun. Hysteresis and creep compensation for piezoelectric actuator in open-loop operation. *Sensors and Actuators A: Physical*, vol. 122, no. 1, pp. 124–130, 2005. DOI: 10.1016/j.sna.2005.03.056.

[21] M. A. Janaideh, M. Rakotondrabe, O. Aliganaideh. Fur-

ther results on hysteresis compensation of smart micropositioning systems with the inverse Prandtlishlinskii-Ishlinskii compensator. *IEEE Transcations on Control Systems Technology*, vol. 24, no. 2, pp. 428–439, 2015. DOI: 10.1109/TCST.2015.2446959.

[22] S. K. Das, H. R. Pota, I. R. Petersen. A MIMO double resonant controller design for nanopositioners. *IEEE Transactions on Nanotechnology*, vol. 14, no. 2, pp. 224–237, 2015. DOI: 10.1109/TNANO.2014.2381274.

[23] W. Li, X. D. Chen. Compensation of hysteresis in piezoelectric actuators without dynamics modeling. *Sensors and Actuators A: Physical*, vol. 199, pp. 89–97, 2013. DOI: 10.1016/j.sna.2013.04.036.

[24] G. Y. Gu, L. M. Zhu, C. Y. Su. Integral resonant damping for high-bandwidth control of piezoceramic stack actuators with asymmetric hysteresis nonlinearity. *Mechatronics*, vol. 24, no. 4, pp. 367–375, 2014. DOI: 10.1016/j.mechatronics.2013.06.001.

[25] L. Riccardi, D. Naso, B. Turchiano, H. Janocha. Design of linear feedback controllers for dynamic systems with hysteresis. *IEEE Transactions on Control Systems Technology*, vol. 22, no. 4, pp. 1268–1280, 2014. DOI: 10.1109/TCST.2013.2282661.

[26] Y. K. Yong, S. O. R. Moheimani, B. J. Kenton, K. K. Leang. Invited review article: High-speed flexure-guided nanopositioning: Mechanical design and control issues. *Review of Scientific Instruments*, vol. 83, no. 12, Article number 121101, 2012. DOI: 10.1063/1.4765048.

[27] G. M. Clayton, S. Tien, K. K. Leang, Q. Z. Zou, S. Devasia. A review of feedforward control approaches in nanopositioning for high-speed SPM. *Journal of Dynamic Systems, Measurement, and Control*, vol. 131, no. 11, Article number 061101, 2009. DOI: 10.1115/1.4000158.

[28] H. Jung, D. G. Gweon. Creep characteristics of piezoelectric actuators. *Review of Scientific Instruments*, vol. 71, no. 4, pp. 1896–1900, 2000. DOI: 10.1063/1.1150559.

[29] K. K. Leang, S. Devasia. Hysteresis, creep, and vibration compensation for piezoactuators: Feedback and feedforward control. *IFAC Proceedings Volumes*, vol. 35, no. 2, pp. 263–269, 2002. DOI: 10.1016/S1474-6670(17)33951-4.

[30] H. M. S. Georgiou, R. Ben Mrad. Dynamic electromechanical drift model for PZT. *Mechatronics*, vol. 18, no. 2, pp. 81–89, 2008. DOI: 10.1016/j.mechatronics.2007.09.005.

[31] G. Y. Gu, L. M. Zhu. High-speed tracking control of piezoelectric actuators using an ellipse-based hysteresis model. *Review of Scientific Instruments*, vol. 81, no. 8, Article number 085104, 2010. DOI: 10.1063/1.3470117.

[32] K. K. Leang, S. Devasia. Feedback-linearized inverse feedforward for creep, hysteresis, and vibration compensation in AFM piezoactuators. *IEEE Transactions on Control Systems Technology*, vol. 15, no. 5, pp. 927–935, 2007. DOI: 10.1109/TCST.2007.902956.

[33] Y. Zhang and P. Yan. Modeling, identification and compensation of hysteresis nonlinearity for a piezoelectric nano-manipulator. *Journal of Intelligent Material Systems and Structures*, vol. 28, no. 7, pp. 907–922, 2017.

[34] F. Preisach. Über die magnetische nachwirkung. *Zeitschrift für physik*, vol. 94, no. 5–6, pp. 277–302, 1935.

[35] M. J. Yang, G. Y. Gu, L. M. Zhu. Parameter identification of the generalized prandtl-ishlinskii model for piezoelectric actuators using modified particle swarm optimization. *Sensors and Actuators A: Physical*, vol. 189, pp. 254–265, 2013. DOI: 10.1016/j.sna.2012.10.029.

[36] Z. Wei, B. L. Xiang, R. X. Ting. Online parameter identification of the asymmetrical Bouc-Wen model for piezoelectric actuators. *Precision Engineering*, vol. 38, no. 4, pp. 921–927, 2014. DOI: 10.1016/j.precisioneng.2014.06.002.

[37] D. Habineza, M. Rakotondrabe, Y. Le Gorrec. Bouc-Wen modeling and feedforward control of multivariable hysteresis in piezoelectric systems: Application to a 3-dof piezotube scanner. *IEEE Transactions on Control Systems Technology*, vol. 23, no. 5, pp. 1797–1806, 2015. DOI: 10.1109/TCST.2014.2386779.

[38] W. Li, X. D. Chen, Z. L. Li. Inverse compensation for hysteresis in piezoelectric actuator using an asymmetric rate-dependent model. *Review of Scientific Instruments*, vol. 84, no. 11, Article number 115003, 2013. DOI: 10.1063/1.4833399.

[39] M. Rakotondrabe. Bouc-Wen modeling and inverse multiplicative structure to compensate hysteresis nonlinearity in piezoelectric actuators. *IEEE Transactions on Automation Science and Engineering*, vol. 8, no. 2, pp. 428–431, 2011. DOI: 10.1109/TASE.2010.2081979.

[40] G. Song, J. Q. Zhao, X. Q. Zhou, J. A. De Abreu-Garcia. Tracking control of a piezoceramic actuator with hysteresis compensation using inverse preisach model. *IEEE/ASME Transactions on Mechatronics*, vol. 10, no. 2, pp. 198–209, 2005. DOI: 10.1109/TMECH.2005.844708.

[41] M. Ruderman, T. Bertram. Discrete dynamic preisach model for robust inverse control of hysteresis systems. In *Proceedings of the 49th IEEE Conference on Decision and Control*, IEEE, Atlanta, USA, pp. 3463–3468, 2010. DOI: 10.1109/CDC.2010.5717758.

[42] J. Zhang, D. Torres, N. Sepúlveda, X. B. Tan. A compressive sensing-based approach for preisach hysteresis model identification. *Smart Materials and Structures*, vol. 25, no. 7, Article number 075008, 2016. DOI: 10.1088/0964-1726/25/7/075008/meta.

[43] B. Song, Z. Sun, N. Xi, R. Yang, Y. Cheng, L. Chen, and L. Dong. Enhanced nonvector space approach for nanoscale motion control. *IEEE Transactions on Nanotechnology*, vol. 17, no. 5, pp. 994–1005, 2018.

[44] D. C. Jiles, D. L. Atherton. Theory of ferromagnetic hysteresis. *Journal of Magnetism and Magnetic Materials*, vol. 61, no. 1-2, pp. 48–60, 1986. DOI: 10.1016/0304-8853(86)90066-1.

[45] S. Rosenbaum, M. Ruderman, T. Strohla, T. Bertram. Use of Jiles-Atherton and preisach hysteresis models for inverse feed-forward control. *IEEE Transactions on Magnetics*, vol. 46, no. 2, pp. 3984–3989, 2010. DOI: 10.1109/TMAG.2010.2071391.

[46] R. C. Smith, Z. Ounaies. A domain wall model for hysteresis in piezoelectric materials. *Journal of Intelligent Material Systems and Structures*, vol. 11, no. 1, pp. 62–79, 2000. DOI: 10.1106/HPHJ-UJ4D-E9D0-2MDY.

[47] A. K. Padthe, B. Drincic, J. Oh, D. D. Rizos, S. D. Fassois, D. S. Bernstein. Duhem modeling of friction-induced hysteresis. *IEEE Control Systems Magazine*, vol. 28, no. 5, pp. 90–107, 2008. DOI: 10.1109/MCS.2008.927331.

[48] X. Wang, V. Pommier-Budinger, Y. Gourinat, A. Reysset. A modified preisach model for hysteresis in piezoelectric actuators. In *Proceedings of the 11th IEEE International Workshop of Electronics, Control, Measurement, Signals and their application to Mechatronics*, IEEE, Toulouse, France, 2013. DOI: 10.1109/ECMSM.2013.6648956.

[49] M. Al Janaideh, S. Rakheja, C. Y. Su. Experimental characterization and modeling of rate-dependent hysteresis of a piezoceramic actuator. *Mechatronics*, vol. 19, no. 5, pp. 656–670, 2009. DOI: 10.1016/j.mechatronics.2009.02.008.

[50] C. Y. Su, Q. Q. Wang, X. K. Chen, and S. Rakheja. Adaptive variable structure control of a class of nonlinear systems with unknown Prandtl-Ishlinskii hysteresis. *IEEE Transactions on Automatic Control*, vol. 50, no. 12, pp. 2069–2074, 2005. DOI: 10.1109/TAC.2005.860260.

[51] G. Y. Gu, L. M. Zhu. Comparative experiments regarding approaches to feedforward hysteresis compensation for piezoceramic actuators. *Smart Materials and Structures*, vol. 23, no. 9, Article number 095029, 2014. DOI: 10.1088/0964-1726/23/9/095029.

[52] G. Y. Gu, L. M. Zhu, C. Y. Su. Modeling and compensation of asymmetric hysteresis nonlinearity for piezoceramic actuators with a modified Prandtl-Ishlinskii model. *IEEE Transactions on Industrial Electronics*, vol. 61, no. 3, pp. 1583–1595, 2014. DOI: 10.1109/TIE.2013.2257153.

[53] Z. Li, C. Y. Su, X. K. Chen. Modeling and inverse adaptive control of asymmetric hysteresis systems with applications to magnetostrictive actuator. *Control Engineering Practice*, vol. 33, pp. 148–160, 2014. DOI: 10.1016/j.conengprac.2014.09.004.

[54] Z. Y. Sun, B. Song, N. Xi, R. G. Yang, L. L. Chen, Y. Cheng, S. Bi, C. J. Li, L. N. Hao. Systematic hysteresis compensator design based on extended unparallel Prandtl-Ishlinskii model for SPM imaging rectification. *IFAC-PapersOnLine*, vol. 50, no. 1, pp. 10901–10906, 2017. DOI: 10.1016/j.ifacol.2017.08.2450.

[55] C. N. Ngoc, P. Bruniaux, J. Castelain, Modeling friction for yarn/fabric simulation application to bending hysteresis. In *Proceedings of the14th European Simulation Symposium*, Dresden, Germany, 2002.

[56] H. Tang, Y. M. Li. Development and active disturbance rejection control of a compliant micro-/nanopositioning piezostage with dual mode. *IEEE Transactions on Industrial Electronics*, vol. 61, no. 3, pp. 1475–1492, 2014. DOI: 10.1109/TIE.2013.2258305.

[57] C. J. Lin, P. T. Lin. Tracking control of a biaxial piezo-actuated positioning stage using generalized duhem model. *Computers & Mathematics with Applications*, vol. 64, no. 5, pp. 766–787, 2012. DOI: 10.1016/j.camwa.2011.12.015.

[58] J. W. Macki, P. Nistri, P. Zecca. Mathematical models for hysteresis. *SIAM Review*, vol. 35, no. 1, pp. 94–123, 1993. DOI: 10.1137/1035005.

[59] J. G. Yi, S. Chang, Y. T. Shen. Disturbance-observer-based hysteresis compensation for piezoelectric actuators. *IEEE/ASME Transactions on Mechatronics*, vol. 14, no. 4, pp. 456–464, 2009. DOI: 10.1109/TMECH.2009.2023986.

[60] C. Y. Su, Y. Stepanenko, J. Svoboda, T. P. Leung. Robust adaptive control of a class of nonlinear systems with unknown backlash-like hysteresis. *IEEE Transactions on Automatic Control*, vol. 45, no. 12, pp. 2427–2432, 2000. DOI: 10.1109/9.895588.

[61] D. B. Ekanayake, R. V. Iyer. Study of a play-like operator. Study of a play-like operator. *Physica B: Condensed Matter*, vol. 403, no. 2–3, pp. 456–459, 2008. DOI: 10.1016/j.physb.2007.08.074.

[62] B. B. Ren, P. P. San, S. S. Ge, T. H. Lee. Adaptive dynamic surface control for a class of strict-feedback nonlinear systems with unknown backlash-like hysteresis. In *Proceedings of American Control Conference*, IEEE, St. Louis, USA, pp. 4482–4487, 2009. DOI: 10.1109/ACC.2009.5160295.

[63] G. Y. Gu, L. M. Zhu, C. Y. Su, H. Ding. Motion control of piezoelectric positioning stages: Modeling, controller design, and experimental evaluation. *IEEE/ASME Transactions on Mechatronics*, vol. 18, no. 5, pp. 1459–1471, 2013. DOI: 10.1109/TMECH.2012.2203315.

[64] G. D. Zhu, H. M. Lei. Adaptive backstepping control of a class of unknown backlash-like hysteresis nonlinear systems. In *Proceedings of the 8th International Conference on Electronic Measurement and Instruments*, IEEE, Xi'an, China, pp. 3–776–3–781, 2007. DOI: 10.1109/ICEMI.2007.4351032.

[65] A. Visintin. *Differential Models of Hysteresis*, Berlin, Heidelberg: Springer, 2013. DOI: 10.1007/978-3-662-11557-2.

[66] Q. S. Xu, P. K. Wong. Hysteresis modeling and compensation of a piezostage using least squares support vector machines. *Mechatronics*, vol. 21, no. 7, pp. 1239–1251, 2011. DOI: 10.1016/j.mechatronics.2011.08.006.

[67] M. Mohammadzaheri, S. Grainger, M. Bazghaleh. Fuzzy modeling of a piezoelectric actuator. *International Journal of Precision Engineering and Manufacturing*, vol. 13, no. 5, pp. 663–670, 2012. DOI: 10.1007/s12541-012-0086-3.

[68] X. L. Zhao, Y. L. Tan. Modeling hysteresis and its inverse model using neural networks based on expanded input space method. *IEEE Transactions on Control Systems Technology*, vol. 16, no. 3, pp. 484–490, 2008. DOI: 10.1109/TCST.2007.906274.

[69] D. Song, C. J. Li. Modeling of piezo actuator's nonlinear and frequency dependent dynamics. *Mechatronics*, vol. 9, no. 4, pp. 391–410, 1999. DOI: 10.1016/S0957-4158(99)00005-7.

[70] G. Y. Gu, L. M. Zhu. Modeling of rate-dependent hysteresis in piezoelectric actuators using a family of ellipses. *Sensors and Actuators A: Physical*, vol. 165, no. 2, pp. 303–309, 2011. DOI: 10.1016/j.sna.2010.09.020.

[71] A. J. Fleming. Charge drive with active DC stabilization for linearization of piezoelectric hysteresis. *IEEE Transactions on Ultrasonics, Ferroelectrics, and Frequency Control*, vol. 60, no. 8, pp. 1630–1637, 2013. DOI: 10.1109/TUFFC.2013.2745.

[72] J. M. Cruz-Hernandez, V. Hayward. Phase control approach to hysteresis reduction. *IEEE Transactions on Control Systems Technology*, vol. 9, no. 1, pp. 17–26, 2001. DOI: 10.1109/87.896742.

[73] S. Bashash, N. Jalili. A polynomial-based linear mapping

strategy for feedforward compensation of hysteresis in piezoelectric actuators. *Journal of Dynamic Systems, Measurement, and Control*, vol. 130, no. 3, Article number 031008, 2008. DOI: 10.1115/1.2907372.

[74] P. Krejc, Hysteresis. Convexity and Dissipation in Hyperbolic Equations. Tokyo: Gakkotosho, 1996.

[75] M. Brokate, J. Sprekels. Hysteresis and phase transitions. Springer Science & Business Media, vol. 121, 2012.

[76] R. Bouc. A mathematical model for hysteresis. *Acta Acustica united with Acustica*, vol. 24, no. 1, pp. 16–25, 1971.

[77] K. Kuhnen, H. Janocha. Compensation of the creep and hysteresis effects of piezoelectric actuators with inverse systems, In *Proceedings of the 6th International Conference on New Actuators*, pp. 309-312, Vancouver, Canada, 2018.

[78] W. S. Galinaitis. Two Methods for Modeling Scalar Hysteresis and Their Use in Controlling Actuators with Hysteresis, Ph.D. dissertation, Virginia Tech, USA, 1999.

[79] S. K. Das, H. R. Pota, I. R. Petersen. Resonant controller design for a piezoelectric tube scanner: A mixed negative-imaginary and small-gain approach. *IEEE Transactions on Control Systems Technology*, vol. 22, no. 5, pp. 1899–1906, 2014. DOI: 10.1109/TCST.2013.2297375.

[80] Q. S. Xu. Identification and compensation of piezoelectric hysteresis without modeling hysteresis inverse. *IEEE Transactions on Industrial Electronics*, vol. 60, no. 9, pp. 3927–3937, 2013. DOI: 10.1109/TIE.2012.2206339.

[81] S. Salapaka, A. Sebastian, J. P. Cleveland, M. V. Salapaka. High bandwidth nano-positioner: A robust control approach. *Review of Scientific Instruments*, vol. 73, no. 9, pp. 3232–3241, 2002. DOI: 10.1063/1.1499533.

[82] P. Ge, M. Jouaneh. Modeling hysteresis in piezoceramic actuators. *Precision Engineering*, vol. 17, no. 3, pp. 211–221, 1995. DOI: 10.1016/0141-6359(95)00002-U.

[83] P. Ge, M. Jouaneh. Generalized preisach model for hysteresis nonlinearity of piezoceramic actuators. *Precision Engineering*, vol. 20, no. 2, pp. 99–111, 1997. DOI: 10.1016/S0141-6359(97)00014-7.

[84] M. J. Jang, C. L. Chen, J. R. Lee. Modeling and control of a piezoelectric actuator driven system with asymmetric hysteresis. *Journal of the Franklin Institute*, vol. 346, no. 1, pp. 17–32, 2009. DOI: 10.1016/j.jfranklin.2008.06.005.

[85] H. W. Ji and Y. Q. Wen. Study on bilinear interpolation preisach model of piezoelectric actuator. *Advanced Materials Research*, vol. 443, pp. 437–441, 2012.

[86] W. T. Ang, P. K. Khosla, C. N. Riviere. Feedforward controller with inverse rate-dependent model for piezoelectric actuators in trajectory-tracking applications. *IEEE/ASME Transactions on Mechatronics*, vol. 12, pp. 134–142, 2007. DOI: 10.1109/TMECH.2007.892824.

[87] T. J. Yeh, H. Ruo-Feng, L. Shin-Wen. An integrated physical model that characterizes creep and hysteresis in piezoelectric actuators. *Simulation Modelling Practice and Theory*, vol. 16, no. 1, pp. 93–110, 2008. DOI: 10.1016/j.simpat.2007.11.005.

[88] Q. S. Xu, Y. M. Li. Dahl model-based hysteresis compensation and precise positioning control of an XY parallel micromanipulator with piezoelectric actuation. *Journal of Dynamic Systems, Measurement, and Control*, vol. 132, no. 4, Article number 041011, 2010. DOI: 10.1115/1.4001712.

[89] P. Z. Li, F. Yan, C. Ge, X. L. Wang, L. S. Xu, J. L. Guo, P. Y. Li. A simple fuzzy system for modelling of both rate-independent and rate-dependent hysteresis in piezoelectric actuators. *Mechanical Systems and Signal Processing*, vol. 36, no. 1, pp. 182–192, 2013. DOI: 10.1016/j.ymssp.2012.10.004.

[90] G. V. Webb, D. C. Lagoudas, A. J. Kurdila. Hysteresis modeling of SMA actuators for control applications. *Journal of Intelligent Material Systems and Structures*, vol. 9, no. 6, pp. 432–448, 1998. DOI: 10.1177/1045389X9800900605.

[91] M. Al Janaideh, M. Rakotondrabe, I. Al-Darabsah, O. Aljanaideh. Internal model-based feedback control design for inversion-free feedforward rate-dependent hysteresis compensation of piezoelectric cantilever actuator. *Control Engineering Practice*, vol. 72, pp. 29–41, 2018. DOI: 10.1016/j.conengprac.2017.11.001.

[92] C. Visone. Hysteresis modelling and compensation for smart sensors and actuators. *Journal of Physics: Conference Series*, vol. 138, Article number 012028, 2008. DOI: 10.1088/1742-6596/138/1/012028.

[93] S. R. Viswamurthy, R. Ganguli. Modeling and compensation of piezoceramic actuator hysteresis for helicopter vibration control. *Sensors and Actuators A: Physical*, vol. 135, no. 2, pp. 801–810, 2007. DOI: 10.1016/j.sna.2006.09.020.

[94] H. Hu, H. M. S. Georgiou, R. Ben-Mrad. Enhancement of tracking ability in piezoceramic actuators subject to dynamic excitation conditions. *IEEE/ASME Transactions on Mechatronics*, vol. 10, no. 2, pp. 230–239, 2005. DOI: 10.1109/TMECH.2005.844705.

[95] R. Venkataraman, P. S. Krishnaprasad. Approximate inversion of hysteresis: Theory and numerical results. In *Proceedings of the 39th IEEE Conference on Decision and Control*, IEEE, Sydney, Australia, pp. 4448–4454, 2000. DOI: 10.1109/CDC.2001.914608.

[96] J. Zhang, Q. M. Yang, C. L. Zhou. £1 adaptive control design for hysteresis compensation within piezoelectric actuators. *IFAC Proceedings Volumes*, vol. 47, no. 3, pp. 2691–2696, 2014. DOI: 10.3182/20140824-6-ZA-1003.02659.

[97] Y. D. Qin, B. Shirinzadeh, Y. L. Tian, D. W. Zhang. Design issues in a decoupled XY stage: Static and dynamics modeling, hysteresis compensation, and tracking control. *Sensors and Actuators A: Physical*, vol. 194, pp. 95–105, 2013. DOI: 10.1016/j.sna.2013.02.003.

[98] G. Y. Gu, L. M. Zhu. An experimental comparison of proportional-integral, sliding mode, and robust adaptive control for piezo-actuated nanopositioning stages. *Review of Scientific Instruments*, vol. 85, no. 5, Article number 055112, 2014. DOI: 10.1063/1.4876596.

[99] S. S. Ge, C. G. Yang, S. L. Dai, T. H. Lee. Adaptive control of a class of strict-feedback discrete-time nonlinear systems with unknown control gains and preceded by hysteresis. In *Proceedings of American Control Conference*, IEEE, St. Louis, USA, pp. 586–591, 2009. DOI: 10.1109/ACC.2009.5160082.

[100] M. C. Deng, C. A. Jiang, A. Inoue. Operator-based robust control for nonlinear plants with uncertain non-symmetric backlash. *Asian Journal of Control*, vol. 13, no. 2,

pp. 317–327, 2011. DOI: 10.1002/asjc.284.

[101] S. H. Bi, M. C. Deng, Y. F. Xiao. Robust stability and tracking for operator-based nonlinear uncertain systems. *IEEE Transactions on Automation Science and Engineering*, vol. 12, no. 3, pp. 1059–1066, 2015. DOI: 10.1109/TASE.2014.2325953.

[102] F. Ikhouane, J. Rodellar. A linear controller for hysteretic systems. *IEEE Transactions on Automatic Control*, vol. 51, no. 2, pp. 340–344, 2006. DOI: 10.1109/TAC.2005.863511.

[103] B. Jayawardhana, H. Logemann, E. P. Ryan. PID control of second-order systems with hysteresis. *International Journal of Control*, vol. 81, no. 8, pp. 1331–1342, 2008. DOI: 10.1080/00207170701772479.

[104] Q. Zheng, F. J. Goforth, A disturbance rejection based control approach for hysteretic systems. In Proceedings of the 49th IEEE Conference on Decision and Control, pp. 3748-3753, Atlanta, USA. DOI: 10.1109/CDE.2010.5717980.

[105] M. Rakotondrabe, Y. Haddab, and P. Lutz. Quadrilateral modelling and robust control of a nonlinear piezoelectric cantilever. *IEEE Transactions on Control Systems Technology*, vol. 17, no. 3, pp. 528–539, 2009. DOI: 10.1109/TCST.2008.2001151.

[106] S. Raafat, R. Akmeliawati, and I. Abdulljabaar. Robust H_∞ controller for high precision positioning system design, analysis, and implementation. *Intelligent Control and Automation*, vol. 3, no. 3, pp. 262–273, 2012. DOI: 10.42361/ica.2012.33030.

[107] H. C. Liaw, B. Shirinzadeh, J. Smith. Enhanced sliding mode motion tracking control of piezoelectric actuators. *Sensors and Actuators A: Physical*, vol. 138, no. 1, pp. 194–202, 2007. DOI: 10.1016/j.sna.2007.04.062.

[108] X. Xue, J. Tang. Robust and high precision control using piezoelectric actuator circuit and integral continuous sliding mode control design. *Journal of Sound and Vibration*, vol. 293, no. 1–2, pp. 335–359, 2006. DOI: 10.1016/j.jsv.2005.10.009.

[109] K. Abidi, A. Sabanovic. Sliding-mode control for high-precision motion of a piezostage. *IEEE Transactions on Industrial Electronics*, vol. 54, no. 1, pp. 629–637, 2007. DOI: 10.1109/TIE.2006.885477.

[110] J. X. Xu, K. Abidi. Discrete-time output integral sliding-mode control for a piezomotor-driven linear motion stage. *IEEE Transactions on Industrial Electronics*, vol. 55, no. 11, pp. 3917–3926, 2008. DOI: 10.1109/TIE.2008.2003194.

[111] J. Y. Peng, X. B. Chen. Integrated PID-based sliding mode state estimation and control for piezoelectric actuators. *IEEE/ASME Transactions on Mechatronics*, vol. 19, no. 1, pp. 88–99, 2014. DOI: 10.1109/TMECH.2012.2222428.

[112] B. Song, Z. Y. Sun, N. Xi, R. G. Yang, L. L. Chen. High precision positioning control for SPM based nanomanipulation: A robust adaptive model reference control approach. In *Proceedings of IEEE/ASME International Conference on Advanced Intelligent Mechatronics*, IEEE, Besacon, France, pp. 1658–1663, 2014. DOI: 10.1109/AIM.2014.6878322.

[113] Y. M. Li, Q. S. Xu. Adaptive sliding mode control with perturbation estimation and PID sliding surface for motion tracking of a piezo-driven micromanipulator. *IEEE Transactions on Control Systems Technology*, vol. 18, no. 4, pp. 798–810, 2010. DOI: 10.1109/TCST.2009.2028878.

[114] X. K. Chen, T. Hisayama. Adaptive sliding-mode position control for piezo-actuated stage. *IEEE Transactions on Industrial Electronics*, vol. 55, no. 11, pp. 3927–3934, 2008. DOI: 10.1109/TIE.2008.926768.

[115] S. Bashash, N. Jalili. Robust adaptive control of coupled parallel piezo-flexural nanopositioning stages. *IEEE/ASME Transactions on Mechatronics*, vol. 14, no. 1, pp. 11–20, 2009. DOI: 10.1109/TMECH.2008.2006501.

[116] H. J. Shieh, C. H. Hsu. An integrator-backstepping-based dynamic surface control method for a two-axis piezoelectric micropositioning stage. *IEEE Transactions on Control Systems Technology*, vol. 15, no. 5, pp. 916–926, 2007. DOI: 10.1109/TCST.2006.890290.

[117] J. H. Zhong, B. Yao. Adaptive robust precision motion control of a piezoelectric positioning stage. *IEEE Transactions on Control Systems Technology*, vol. 16, no. 5, pp. 1039–1046, 2008. DOI: 10.1109/TCST.2007.916319.

[118] H. C. Liaw, B. Shirinzadeh. Robust adaptive constrained motion tracking control of piezo-actuated flexure-based mechanisms for micro/nano manipulation. *IEEE Transactions on Industrial Electronics*, vol. 58, no. 4, pp. 1406–1415, 2011. DOI: 10.1109/TIE.2010.2050413.

[119] Q. Xu and Y. Li. Micro/nanopositioning using model predictive output integral discrete sliding mode control. *IEEE Transactions on Industrial Electronics*, vol. 59, pp. 1161–1170, 2012. DOI: 10.1109/TIE.2011.2157287.

[120] V. A. Neelakantan, G. N.Washington, and N. K. Bucknor. Model predictive control of a two stage actuation system using piezoelectric actuators for controllable industrial and automotive brakes and clutches. *Journal of Intelligent Material Systems and Structures*, vol. 19, no. 7, pp. 845–857, 2008.

[121] G. S. Choi, Y. A. Lim, G. H. Choi. Tracking position control of piezoelectric actuators for periodic reference inputs. *Mechatronics*, vol. 12, no. 5, pp. 669–684, 2002. DOI: 10.1016/S0957-4158(01)00020-4.

[122] M. Altaher and S. S. Aphale. High-precision control of a piezo-driven nanopositioner using fuzzy logic controllers. *Computers*, vol. 7, no. 1, Article number 10, 2018. DOI: 10.3390/computers7010010.

[123] A. Sebastian and S. M. Salapaka. Design methodologies for robust nano-positioning. *IEEE Transactions on Control Systems Technology*, vol. 13, no. 6, pp. 868–876, 2005. DOI: 10.1109/TCST.2005.854336.

[124] R. J. E. Merry, J. L. Holierhoek, M. J. G. van de Molengraft, M. Steinbuch. Gain scheduling control of a walking piezo actuator. *IEEE/ASME Transactions on mechatronics*, vol. 19, no. 3, pp. 954–962, 2014. DOI: 10.1109/TMECH.2013.2264834.

[125] M. S. Tsai, J. S. Chen. Robust tracking control of a piezo-actuator using a new approximate hysteresis model. *Journal of Dynamic Systems, Measurement, and Control*, vol. 125, no. 1, pp. 96–102, 2003. DOI: 10.1115/1.1540114.

[126] S. S. Ku, U. Pinsopon, S. Cetinkunt, S. Nakajima. Design, fabrication, and real-time neural network control of a three-degrees-of-freedom nanopositioner. *IEEE/ASME Transactions on Mechatronics*, vol. 5, no. 3, pp. 273–280, 2000. DOI: 10.1109/3516.868919.

[127] F. J. Lin, R. J. Wai, K. K. Shyu, T. M. Liu. Recurrent fuzzy neural network control for piezoelectric ceramic linear ultrasonic motor drive. *IEEE Transactions on Ultrasonics, Ferroelectrics, and Frequency Control*, vol. 48, no. 4, pp. 900–913, 2001. DOI: 10.1109/58.935707.

[128] H. C. Liaw, B. Shirinzadeh. Neural network motion tracking control of piezo-actuated flexure-based mechanisms for micro-/nanomanipulation. *IEEE/ASME Transactions on Mechatronics*, vol. 14, no. 5, pp. 517–527, 2009. DOI: 10.1109/TMECH.2009.2005491.

[129] C. M. Lin, H. Y. Li. Intelligent control using the wavelet fuzzy cmac backstepping control system for two-axis linear piezoelectric ceramic motor drive systems. *IEEE Transactions on Fuzzy Systems*, vol. 22, no. 4, pp. 791–802, 2014. DOI: 10.1109/TFUZZ.2013.2272648.

[130] C. M. Wen, M. Y. Cheng. Development of a recurrent fuzzy CMAC with adjustable input space quantization and self-tuning learning rate for control of a dual-axis piezoelectric actuated micromotion stage. *IEEE Transactions on Industrial Electronics*, vol. 60, no. 11, pp. 5105–5115, 2013. DOI: 10.1109/TIE.2012.2221114.

[131] J. X. Xu, D. Q. Huang, V. Venkataramanan, T. C. T. Huynh. Extreme precise motion tracking of piezoelectric positioning stage using sampled-data iterative learning control. In *Proceedings of the 37th Annual Conference of the IEEE Industrial Electronics Society*, IEEE, Melbourne, Australia, pp. 3376–3381, 2011. DOI: 10.1109/IECON.2011.6119854.

[132] H. R. P. Sajal K. Das and I. R. Petersen, Minimax lqg controller design for nanopositioners, In *Proceedings of the European Control Conference*, , Strasbourg, France, pp. 1933-1938, 2014. DOI: 10.1109/ECC.2014.6862321.

[133] Y. Shen, E. Winder, N. Xi, C. A. Pomeroy, and U. C. Wejinya. Closed-loop optimal control-enabled piezoelectric microforce sensors. *IEEE/ASME Transactions on Mechatronics*, vol. 11, no. 4, pp. 420–427, 2006.

[134] S. Kuiper, G. Schitter. Active damping of a piezoelectric tube scanner using self-sensing piezo actuation. *Mechatronics*, vol. 20, no. 6, pp. 656–665, 2010. DOI: 10.1016/j.mechatronics.2010.07.003.

[135] Y. F. Liu, J. J. Shan. Feedback/feedforward control of hysteresis-compensated piezoactuators for highspeed scanning applications. In *Proceedings of the 23rd IEEE International Symposium on Industrial Electronics*, IEEE, Istanbul, Turkey, pp. 281–286, 2014. DOI: 10.1109/ISIE.2014.6864625.

[136] M. Rakotondrabe, K. Rabenorosoa, J. Agnus, N. Chaillet. Robust feedforward-feedback control of a nonlinear and oscillating 2-DOF piezocantilever. *IEEE Transactions on Automation Science and Engineering*, vol. 8, no. 3, pp. 506–519, 2011. DOI: 10.1109/TASE.2010.2099218.

[137] S. K. Das, F. R. Badal, A. Rahman, A. Islam, S. K. Sarker, N. Paul. Improvement of alternative non-raster scanning methods for high speed atomic force microscopy: A review. *IEEE Access*, vol. 7, pp. 115603–115624, 2019. DOI: 10.1109/ACCESS.2019.2936471.

[138] S. Devasia, E. Eleftheriou, S. O. R. Moheimani. A survey of control issues in nanopositioning. *IEEE Transactions on Control Systems Technology*, vol. 15, no. 5, pp. 802–823, 2007. DOI: 10.1109/TCST.2007.903345.

[139] Y. F. Shan, K. K. Leang. Accounting for hysteresis in repetitive control design: Nanopositioning example. *Automatica*, vol. 48, no. 8, pp. 1751–1758, 2012. DOI: 10.1016/j.automatica.2012.05.055.

[140] I. Ahamd, A. M. Abdurraqeeb. H_∞ control design with feed-forward compensator for hysteresis compensation in piezoelectric actuators. *Automatika*, vol. 57, no. 3, pp. 691–702, 2016. DOI: 10.7305/automatika.2017.02.1786.

[141] Y. Cao, L. Cheng, X. B. Chen, J. Y. Peng. An inversion-based model predictive control with an integral-of-error state variable for piezoelectric actuators. *IEEE/ASME Transactions on Mechatronics*, vol. 18, no. 3, pp. 895–904, 2013. DOI: 10.1109/TMECH.2012.2194792.

[142] G. Y. Gu, L. M. Zhu, C. Y. Su. High-precision control of piezoelectric nanopositioning stages using hysteresis compensator and disturbance observer. *Smart Materials and Structures*, vol. 23, no. 10, Article number 105007, 2014. DOI: 10.1088/0964-1726/23/10/105007.

[143] U. X. Tan, W. T. Latt, F. Widjaja, C. Y. Shee, C. N. Riviere, W. T. Ang. Tracking control of hysteretic piezoelectric actuator using adaptive rate-dependent controller. *Sensors and Actuators A: Physical*, vol. 150, no. 1, pp. 116–123, 2009. DOI: 10.1016/j.sna.2008.12.012.

[144] J. C. Shen, W. Y. Jywe, H. K. Chiang, Y. L. Shu. Precision tracking control of a piezoelectric-actuated system. *Precision Engineering*, vol. 32, no. 2, pp. 71–78, 2008. DOI: 10.1016/j.precisioneng.2007.04.002.

[145] G. Y. Gu, L. M. Zhu. Motion control of piezoceramic actuators with creep, hysteresis and vibration compensation. *Sensors and Actuators A: Physical*, vol. 197, pp. 76–87, 2013. DOI: 10.1016/j.sna.2013.03.005.

[146] J. M. Rodriguez-Fortun, J. Orus, J. Alfonso, F. B. Gimeno, J. A. Castellanos. Flatness-based active vibration control for piezoelectric actuators. *IEEE/ASME Transactions on Mechatronics*, vol. 18, no. 1, pp. 221–229, 2013. DOI: 10.1109/TMECH.2011.2166998.

[147] T. C. Tsao, M. Tomizuka. Adaptive zero phase error tracking algorithm for digital control. *Journal of Dynamic Systems, Measurement, and Control*, vol. 109, no. 4, pp. 349–354, 1987. DOI: 10.1115/1.3143866.

[148] J. A. Butterworth, L. Y. Pao, D. Y. Abramovitch. Analysis and comparison of three discrete-time feedforward model-inverse control techniques for nonminimum-phase systems. *Mechatronics*, vol. 22, no. 5, pp. 577–587, 2012. DOI: 10.1016/j.mechatronics.2011.12.006.

[149] J. A. Butterworth, L. Y. Pao, D. Y. Abramovitch. A comparison of control architectures for atomic force microscopes. *Asian Journal of Control*, vol. 11, no. 2, pp. 175–181, 2009. DOI: 10.1002/asjc.93.

[150] S. S. Aphale, S. Devasia, S. O. R. Moheimani. High-bandwidth control of a piezoelectric nanopositioning stage in the presence of plant uncertainties. *Nanotechnology*, vol. 19, no. 12, Article number 125503, 2008. DOI: 10.1088/0957-4484/19/12/125503.

[151] Y. Li, J. Bechhoefer. Feedforward control of a closed-loop piezoelectric translation stage for atomic force microscope. *Review of Scientific Instruments*, vol. 78, no. 1, Article number 013702, 2007. DOI: 10.1063/1.2403839.

[152] G. Wang, G. Q. Chen, F. Z. Bai. High-speed and precision control of a piezoelectric positioner with hysteresis, resonance and disturbance compensation. *Microsystem Technologies*, vol. 22, no. 10, pp. 2499–2509, 2016. DOI:

10.1007/s00542-015-2638-9.

[153] G. Y. Gu, M. J. Yang, L. M. Zhu. Real-time inverse hysteresis compensation of piezoelectric actuators with a modi_ed prandtl-ishlinskii model. *Review of Scientic Instruments*, vol. 83, no. 6, Article number 062106, 2012. DOI: 10.1063/1.4728575.

[154] M. J. Yang, G. Y. Gu, and L.M. Zhu. High-bandwidth tracking control of piezo-actuated nanopositioning stages using closed-loop input shaper. *Mechatronics*, vol. 24, no. 6, pp. 724–733, 2014. DOI: 10.1016/j.mechatronics.2014.02.014.

[155] H. Habibullah, H. R. Pota, I. R. Petersen. A novel control approach for high-precision positioning of a piezoelectric tube scanner. *IEEE Transactions on Automation Science and Engineering*, vol. 14, no. 1, pp. 325–336, 2017. DOI: 10.1109/TASE.2016.2526641.

[156] J. C. Shen, W. Y. Jywe, C. H. Liu, Y. T. Jian, J. Yang. Sliding-mode control of a three-degrees-of-freedom nanopositioner. *Asian Journal of Control*, vol. 10, no. 3, pp. 267–276, 2008. DOI: 10.1002/asjc.33.

[157] S. Polit, J. Dong. Development of a highbandwidth xy nanopositioning stage for high-rate micro-nanomanufacturing. *Asian Journal of Control*, vol. 16, pp. 724–733, 2011. DOI: 10.1109/TMECH.2010.2052107.

[158] A. Oliveri, M. Lodi, M. Parodi, F. Stellino, M. Storace. Model reduction for optimized online compensation of hysteresis and creep in piezoelectric actuators. *IEEE Transactions on Circuits and Systems II: Express Briefs*, vol. 65, no. 11, pp. 1748–1752, 2017. DOI: 10.1109/TCSII.2017.2767287.

[159] Z. Y. Sun, L. N. Hao, B. Song, R. G. Yang, R. M. Cao, Y. Cheng. Periodic reference tracking control approach for smart material actuators with complex hysteretic characteristics. *Smart Materials and Structures*, vol. 25, no. 10, Article number 105029, 2016. DOI: 10.1088/0964-1726/25/10/105029/meta.

[160] S. M. Salapaka, M. V. Salapaka. Scanning probe microscopy. Scanning probe microscopy. *IEEE Control Systems Magazine*, vol. 28, no. 2, pp. 65–83, 2008. DOI: 10.1109/MCS.2007.914688.

[161] Y. Tian, D. Zhang, B. Shirinzadeh. Dynamic modelling of a flexure-based mechanism for ultra-precision grinding operation. *Precision Engineering*, vol. 35, no. 4, pp. 554–565, 2011. DOI: 10.1016/j.precisioneng.2011.03.001.

[162] Y. M. Li, Q. S. Xu. A totally decoupled piezo-driven XYZ flexure parallel micropositioning stage for micro/nanomanipulation. *IEEE Transactions on Automation Science and Engineering*, vol. 8, no. 2, pp. 265–279, 2011. DOI: 10.1109/TASE.2010.2077675.

[163] M. A. Rahman, A. Al Mamun, K. Yao, S. K. Das. Design and implementation of feedback resonance compensator in hard disk drive servo system: A mixed passivity, negative-imaginary and small-gain approach in discrete time. *Journal of Control, Automation and Electrical Systems*, vol. 26, no. 4, pp. 390–402, 2015. DOI: 10.1007/s40313-015-0189-z.

[164] M. Armin, P. N. Roy, S. K. Sarkar, S. K. Das. LMI-based robust PID controller design for voltage control of islanded microgrid. *Asian Journal of Control*, vol. 20, no. 5, pp. 2014–2025, 2018. DOI: 10.1002/asjc.1710.

[165] G. Baruah, S. Majhi, C. Mahanta. Auto-tuning of FOPI controllers for TITO processes with experimental validation. *International Journal of Automation and Computing*, vol. 16, no. 5, pp. 589–603, 2019. DOI: 10.1007/s11633-018-1140-0.

[166] O. Yahya, Z. Lassoued, K. Abderrahim. Predictive control based on fuzzy supervisor for PWARX hybrid model. *International Journal of Automation and Computing*, vol. 16, no. 5, pp. 683–695, 2019. DOI: 10.1007/s11633-018-1148-5.

[167] Y. Xu, T. Shen, X. Y. Chen, L. L. Bu, N. Feng. Predictive adaptive Kalman filter and its application to INS/UWB-integrated human localization with missing UWB-based measurements. *International Journal of Automation and Computing*, vol. 16, no. 5, pp. 604–613, 2019. DOI: 10.1007/s11633-018-1157-4.

Maniza Armin received the B. Sc. degree in mechatronics engineering from Rajshahi University of Engineering & Technology (RUET), Bangladesh. She is currently working on robust control of both smart grid and microgrid.

Her research interests include control applications, power system control, IoT and robotics.

E-mail: maniza.13.mte@gmail.com (Corresponding author)
ORCID iD: 0000-0002-4332-1731

Priyo Nath Roy received the B. Sc. degree in mechatronics engineering from Rajshahi University of Engineering & Technology, Bangladesh. In July 2019, he joined in the Department of Mechatronics Engineering of Khulna University of Engineering & Technology, Bangladesh as a Lecturer. He is currently working on robust control of both smart grid and microgrid.

His research interests include control applications, power system control, IoT and robotics.

E-mail: priyo1124@gmail.com

Sajal Kumar Das received the Ph. D. degree in electrical engineering from University of New South Wales, Australia on 2014. In May 2014, he was appointed as a research engineer in National University of Singapore degree, Singapore. In January 2015, he joined in the Department of Electrical and Electronic Engineering, American International University-Bangladesh (AIUB), Bangladesh as an assistant professor. He continued his work at AIUB until he joined in the Department of Mechatronics Engineering, Rajshahi University of Engineering & Technology (RUET), Bangladesh as a lecturer on September 2015. He is currently working as an assistant professor in RUET.

His research interests include control theory and applications, mechatronics system control, robotics, and power system control.

E-mail: das.k.sajal@gmail.com